MOLECULAR AND CELLULAR BIOLOGY, Feb. 2011, p. 845–860 Vol. 31, No. 4
0270-7306/11/$12.00 doi:10.1128/MCB.00159-10

HBO1 Is Required for H3K14 Acetylation and Normal Transcriptional Activity during Embryonic Development[▽]

Andrew J. Kueh,[1,2] Mathew P. Dixon,[1] Anne K. Voss,[1,2]†* and Tim Thomas[1,2]†*

The Walter and Eliza Hall Institute of Medical Research, Parkville, Victoria 3050, Australia,[1] and Department of Medical Biology, The University of Melbourne, Parkville, Victoria 3050, Australia[2]

Received 9 February 2010/Returned for modification 15 March 2010/Accepted 3 December 2010

We report here that the MYST histone acetyltransferase HBO1 (histone acetyltransferase bound to ORC; MYST2/KAT7) is essential for postgastrulation mammalian development. Lack of HBO1 led to a more than 90% reduction of histone 3 lysine 14 (H3K14) acetylation, whereas no reduction of acetylation was detected at other histone residues. The decrease in H3K14 acetylation was accompanied by a decrease in expression of the majority of genes studied. However, some genes, in particular genes regulating embryonic patterning, were more severely affected than "housekeeping" genes. Development of HBO1-deficient embryos was arrested at the 10-somite stage. Blood vessels, mesenchyme, and somites were disorganized. In contrast to previous studies that reported cell cycle arrest in HBO1-depleted cultured cells, no defects in DNA replication or cell proliferation were seen in *Hbo1* mutant embryo primary fibroblasts or immortalized fibroblasts. Rather, a high rate of cell death and DNA fragmentation was observed in *Hbo1* mutant embryos, resulting initially in the degeneration of mesenchymal tissues and ultimately in embryonic lethality. In conclusion, the primary role of HBO1 in development is that of a transcriptional activator, which is indispensable for H3K14 acetylation and for the normal expression of essential genes regulating embryonic development.

In general, acetylation of histone lysine residues correlates positively and strongly with transcriptionally active regions of the genome (37, 49, 54); in contrast, heterochromatin is hypoacetylated (7, 8). It has been proposed that particular patterns of posttranslational histone modifications represent a "code" and that histone modifications are recognized by transcription factors via specific chromatin-binding domains (2, 31, 60, 68). Indeed, acetylated lysines are recognized by bromodomains (13, 30). However, histones can be acetylated at multiple sites, and with few exceptions, very little is known about the biological function of acetylation at specific histone lysine residues in multicellular organisms. Moreover, the residue specificity of few histone acetyltransferases has been characterized in vertebrate organisms. Two members of the MYST family of histone acetyltransferases, MOF (MYST1/KAT8) and MOZ (MYST3/KAT6A), have highly restricted substrate specificities *in vivo*. In *Drosophila melanogaster* and mice *in vivo*, as well as in human cells *in vitro*, MOF is specifically required for acetylation of histone 4 lysine 16 (H4K16) (3, 61, 64), whereas MOZ has a specific role in the acetylation of H3K9 in *Hox* gene clusters (69). Since embryonic development is dependent on the precise regulation of temporal-spatial patterns of gene expression, establishing the correct pattern of histone acetylation at developmentally important gene loci is critical. Accordingly, MOF and MOZ, as well two other MYST family members, QKF (MORF/MYST4/KAT6B) and TIP60 (KAT5), have distinct and essential functions during mammalian development (21, 24, 34, 47, 63, 64, 67, 69). We show here that the MYST histone acetyltransferase HBO1 is required for the expression of a broad range of genes and is essential for the acetylation of H3K14.

HBO1 was originally identified in a screen for proteins interacting with origin recognition complex protein 1 (ORC1) (28). The assembly of ORC, along with CDC6/CDC18, CDT1, and MCM2 to -7, onto replication origins forms the prereplication complex, which confers a license for the initiation of DNA replication and ensures that DNA is replicated only once per cell cycle (41). Apart from this interaction with ORC1, HBO1 has also been shown to associate with other prereplication complex subunits. For instance, the zinc finger of HBO1 can interact with MCM2 in cervical carcinoma cells (9), and the depletion of XHbo1 in *Xenopus laevis* egg extracts has been reported to disrupt chromatin binding of Mcm2 to -7, resulting in an abolishment of DNA replication activity (26). Furthermore, the knockdown of HBO1 using RNA interference (RNAi) in preadipocytes appears to repress mitotic clonal expansion and adipogenesis, leading to the conclusion that HBO1 acts together with Fad24 to promote adipogenesis by regulating DNA replication (32). More recently, HBO1 has been reported to interact directly with CDT1, where it enhances CDT1-dependent re-replication, and thus HBO1 is proposed to act as a coactivator of CDT1 at replication origins (44). Together, these findings strongly suggest that the primary function of HBO1 is associated with DNA replication.

It has been reported that the acetyltransferase activity of HBO1 is involved in many of its replication-associated functions. HBO1 has been shown to acetylate prereplication complex components, such as ORC2, MCM2, and CDC6, in cell-free acetylation assays, and its histone acetyltransferase activity is reported to be specifically upregulated during G_2/M phase of

* Corresponding author. Mailing address: The Walter and Eliza Hall Institute of Medical Research, Parkville, Victoria 3050, Australia. Phone for Anne K. Voss: 61 3 9345 2642. Fax: 61 3 9347 0852. E-mail: avoss@wehi.edu.au. Phone for Tim Thomas: 61 3 9345 2642. Fax: 61 3 9347 0852. E-mail: tthomas@wehi.edu.au.

† These authors jointly supervised the project and contributed equally.

▽ Published ahead of print on 13 December 2010.

the cell cycle in adenocarcinoma epithelial cells (26). In cell-free histone acetyltransferase assays, HBO1 acetylates recombinant *Xenopus* nucleosome core particles at H4K5, H4K8, and H4K12 residues (14). These cell-free acetylation assays suggest that HBO1 is a broad-spectrum acetyltransferase and may have a wide variety of both histone and nonhistone targets.

Apart from its proposed role in DNA replication within ORC, there is evidence that HBO1 is involved in transcriptional regulation. HBO1 colocalizes with a multisubunit histone acetyltransferase complex consisting of ING4/5, hEaf6, and JADE1/2/3, in which PHD fingers on ING4/5 and JADE1/2/3 subunits confer targeting of the complex to chromatin by binding methylated histone lysine residues (51). JADE1 can alternatively be spliced into two splice variants, JADE1L and JADE1S. Interestingly, JADE1S complexes contain HBO1 and hEaf6 but not ING4/5, resulting in a preferential shift from binding methylated H3K4 to binding methylated H3K36 residues. Correspondingly, ING4/5 and JADE1S complexes have been hypothesized to regulate transcriptional initiation and elongation, respectively, based on the finding that HBO1 and its associated subunits colocalize on transcriptional start sites and gene coding regions in HeLa cells (51). Additionally, the MYST domain of HBO1 is involved in enhancing progesterone receptor transcriptional activity in monkey CV1 kidney cells (18). The *Drosophila* homologue of HBO1, chameau, can genetically interact with polycomb group proteins to mediate *Hox* gene silencing, indicating a role in transcriptional repression (20). On the other hand, chameau can also act downstream of DFos and DJun in transcriptional activation (42). Furthermore, the serine-rich N terminus of HBO1 represses androgen receptor- and NF-κB-mediated transcriptional activation in CV1 and 293T cells, respectively (11, 57).

These studies suggest that HBO1 is a multifunctional protein that may be required for DNA replication as well as promoting and repressing transcription by virtue of its activity in acetylating a wide range of targets.

In order to examine the function of HBO1 during mammalian development, we have created an *Hbo1* null allele. Utilizing a series of cell proliferation and DNA replication assays, we show *in vivo* and *in vitro* that HBO1 is not essential for DNA replication or cell proliferation. Importantly, we report that the primary biological function of HBO1 is to mediate H3K14 acetylation and that HBO1 acts as an essential activator of gene expression during postgastrulation embryonic development.

MATERIALS AND METHODS

Generation of the *Hbo1* mutant allele. A targeting construct was produced using a 9.3-kb fragment from the bacterial artificial chromosome RP23-480C5, which contains the entire *Hbo1* gene. A *loxP* site was introduced 492 bp 5′ of exon 1, and a *Neo* cassette, flanked by *FRT* sites and also containing a single *loxP* site at the 3′ end, was introduced between exons 1 and 2 using the recombineering method (39). After electroporation into C57BL/6 embryonic stem (ES) cells, screening of 272 clones yielded 8 correctly targeted cell lines. The *Neo* cassette together with exon 1 was removed by crossing heterozygous mice to a cre-recombinase deleter strain (55). This resulted in a mouse strain in which bases 687 bp 5′ and bases 781 bp 3′ of the start point of translation, including exon 1, have been deleted. A single *loxP* site remains 5′ of exon 2. PCR genotyping using 3 oligonucleotides allowed the identification of $Hbo1^{+/+}$, $Hbo1^{lox/lox}$, $Hbo1^{+/-}$, and $Hbo1^{-/-}$ genotypes. Amplification of the wild-type and floxed alleles using oligonucleotide "1" (TAAGAGCTATTCCGTGTTCCGG) and oligonucleotide "2" (AACTGGAAATTCTTTGGCGCTCC) resulted in products of 190 and 283 bases, respectively. Amplification of the null allele using oligonucleotide "1" and oligonucleotide "3" (ATCAATTCTGCCTGGCTTAACCC) resulted in a product of 358 bases (see Fig. 1B).

TABLE 1. cDNA templates for cRNA probes

Gene	Source	Clone corresponds to:
Hoxa2	Generated by PCR (GenBank accession no. NM10451)	Bases 257-1461
Hoxa3	Generated by PCR (GenBank accession no. Y11717)	Bases 741-1759
Gata4	L. Robb	490-bp cDNA fragment
Erg	T. Willson	Full-length coding region
Otx2	L. Robb	1-kb cDNA fragment
Sox2	L. Robb	775-bp cDNA fragment
Shh	L. Robb	640-bp cDNA fragment
Hbo1	Generated by PCR (GenBank accession no. NM_177619)	Bases 292-1337

Mice were fed *ad libitum* and housed under a 12-h light/dark cycle. Experimental animals were backcrossed onto an F1 hybrid background of the strains FVB and BALB/c. For timed matings, females were housed with stud males, checked after 2 h for the presence of a vaginal plug, and then left to mate overnight. Mice were considered to be 0.5 days pregnant at midday if a vaginal plug was observed in the morning of the same day but was not present the previous evening. Experiments were undertaken with the approval of the Royal Melbourne Research Foundation Animal Ethics Committee.

$Hbo1^{-/-}$ embryos were stage matched to control embryos by somite count in experiments with results depicted in Fig. 2K to R, Fig. 3I to L, Fig. 4A to R, Fig. 5A to P, and Fig. 7A to F. $Hbo1^{-/-}$ embryos with excessively degenerated somites were not used.

Antibodies. Antibodies used were raised against GCN5 (1:500, AB18381), HBO1 (1:500, AB37289), acetylated H4K12 (1:500, AB1761), and MCM2 (1:200, AB31159), purchased from Abcam; bromodeoxyuridine (BrdU) (1:10, M0744), purchased from Dako; HIF-1α (1:20, MAB1935), purchased from R&D Systems; CD31 (1:250, 557355), purchased from BD Pharmingen; nidogen (1:200), a gift from Marie Dziadek; acetylated H4K5 (1:2,000, 07-327), acetylated H4K8 (1:2,000, 07-328), acetylated H4K16 (1:2,000, 07-329), acetylated H3K9 (1:2,000, 07-352), and acetylated H3K14 (1:2,000, 070353), purchased from Upstate; and actin (1:2,000, sc-1616 horseradish peroxidase [HRP]), purchased from Santa Cruz. BrdU labeling, terminal deoxynucleotidyltransferase-mediated dUTP-biotin nick end labeling (TUNEL) staining, immunohistochemistry, and Western blotting were performed as described previously (67, 70).

Analysis of gene expression and chromatin immunoprecipitation (ChIP). Whole-mount and radioactive RNA *in situ* hybridization experiments were conducted as described previously (66, 72). *Hbo1* mRNA was detected using a 1-kb probe corresponding to exons 4 to 12 of the *Hbo1* gene. Northern blot analysis was performed using the same 1-kb *Hbo1* probe. *In situ* hybridization probes *Nkx2.5* (4), *Tbx1* (10), *Vegfa* (72), *Flk-1* (62), *Tie-1* (35), *Tie-2* (53), *Hex* (62), *Notch1* (46), *brachyury* (74), and *Hsp90ab1* (72) have been previously described; other probes are listed in Table 1.

For reverse transcriptase quantitative PCR (RT-qPCR) analysis for gene expression, RNA was purified using RNA extraction columns (RNeasy minikit; Qiagen) with an on-column DNase digest. For all samples, 1 μg of the extracted RNA was used as a template to generate cDNA. Quantitative PCR methodology and subsequent data analysis have been described previously (69). Primer sequences are listed in Table 2.

For ChIP experiments, fragmented chromatin was prepared from embryos using a chromatin prep kit (EZ-Zyme; Millipore), and subsequent immunoprecipitation steps were conducted using a chromatin immunoprecipitation kit (EZ-Magna ChIP; Millipore). Quantitative PCR methodology and data analysis have been described previously (69). Primer sequences are listed in Table 3.

Cell culture. For the embryonic day 3.5 (E3.5) outgrowth assay, uteri of pregnant mice were flushed at E3.5, and embryos were collected and subsequently cultured in ES cell medium as described previously (71). Cultures were photographed daily.

For the MTT [3-(4,5-dimethyl-2-thiazolyl)-2,5-diphenyl-2H-tetrazolium bromide] fibroblast proliferation assay, embryos were dissected at E9.5 and mechanically dissociated by gentle pipetting before being cultured in fibroblast growth medium (10% fetal calf serum [FCS], 2 mM L-glutamine, 100 IU/ml penicillin, and 0.1 mg/ml streptomycin in high-glucose Dulbecco's modified Eagle's medium

TABLE 2. RT-qPCR primers

Target gene	Primer sequence 5′	Primer sequence 3′	Primer position bp[a]	Primer position Exon(s)	NCBI accession no.
B-actin	AAGGCCAACCGTGAAAAGAT	GTGGTACGACCAGAGGCATAC	+336	3–4	NM_007393.3
brachyury	GAAGGCGCCTGTGTCTTTC	CCCCCAACTCTCACGATG	+415	2–3	NM_009309.2
Flk-1	CCCCATTTCAATGGAGAAAC	TAGGCGAGATCAAGGCTTTC	+1211	9–10	NM_010612.2
Gcn5	AGAGGAAGGCGCAAGTCC	TCCAGCCATTACACTTGCAG	+250	1–2	NM_001038010.2
Hbo1	TTTTGGCCGCTATGAACTG	GGAGGATTGTCTGGCTCTTC	+755	8	NM_001195004.1
Hoxa3	ATGGGACCCCACACTTACAG	GTGTGGGGGAGGTGAGTTAG	+1066	5	NM_010452.3
Hsp90ab1	ACCTGGGAACCATTGCTAAG	AGAATCCGACACCAAACTGC	+301	3–4	NM_008302.3
Mof	CTCGAAACCAAAAGCGAAAG	CCTCGTGTTCCTTTTCCAAG	+415	3–4	NM_026370.1
Moz	GTCGTGACCAAGGCAAAAAC	GGGTCACAACACTCCATGTG	+802	5–6	NM_001081149.1
Notch1	TCAGGGTGTCTTCCAGATCC	AGCCAGGATCAGTGGAGTTG	+5888	31–32	NM_008714.3
Otx2	GAATCCAGGGTGCAGGTATG	TTCTGACCTCCATTCTGCTG	+234	2–3	NM_144841.3
Pgk1	TACCTGCTGGCTGGATGG	CACAGCCTCGGCATATTTCT	+919	8–9	NM_008828.2
Psmb2	GAGGGCAGTGGAGCTTCTTA	AGGTGGGCAGATTCAAGATG	+461	5–6	NM_011970.4
Rpl13a	GGAGAAACGGAAGGAAAAGG	TGAGGACCTCTGTGAACTTGC	+470	7–8	NM_009438.4
Sox1	AACCCCAAGATGCACAACTC	TGTAATCCGGGTGTTCCTTC	+216	1	NM_009233.3
Sox2	CTCTGCACATGAAGGAGCAC	CCGGGAAGCGTGTACTTATC	+301	1	NM_011443.3
Tbx1	GTGGACCCTCGAAAAGACAG	GATCCGGTGATTCTGGTAGG	+729	4–5	NM_011532.1
Tie-1	CCGAAGAAGCTGCCTACATC	TCAAGGTCCCTGAGCTGAAC	+2345	14–15	NM_011587.2
Tie-2	TCCGAGCTAGAGTCAACACC	CTGGTTGAGGAGGGAGAATG	+1834	12–13	NM_013690.2

[a] Position on cDNA sequence downstream of ATG.

[DMEM]). Derived primary embryonic fibroblasts (PEFs) were trypsinized, and 1,000 cells from each culture were plated in triplicate in 96-well plates. To quantify cell number, 4 μg of MTT was added to each sample, and samples were left to incubate for 2 h. Culture medium was replaced by dimethyl sulfoxide (DMSO), samples were mixed thoroughly, and absorbance readings were measured using a plate reader (Genios; Tecan).

For fluorescence-activated cell sorter (FACS) analysis for cell cycle distribution, E9.5-derived primary embryonic fibroblasts were fixed in 70% ethanol overnight, washed twice in phosphate-buffered saline (PBS), stained with 20 μg/ml propidium iodide for 20 min at room temperature, and analyzed using a FACSCalibur instrument. Cell cycle analysis was performed using FlowJo software.

For the tamoxifen-induced-deletion assay, $Hbo1^{lox/lox}$ mice were crossed to $Hbo1^{lox/+}$ mice carrying the Cre-ERT transgene (22). Embryos were dissected at E10.5, cultured in fibroblast growth medium, and repeatedly passaged over 10 weeks to select for immortalized cells. Cultures were then treated with 0.5 μM 4OH-tamoxifen (1,000× stock in 100% ethanol; Sigma) for 24 h to induce cre recombination and *Hbo1* deletion. Cell lines were continuously passaged once a week for 15 weeks in the absence of tamoxifen and were genotyped every 5 weeks to assess the viability of *Hbo1*-deleted cells.

Transplacental uptake assay. Pregnant female mice were injected intraperitoneally with a bolus of 100 μl (10 μCi) of [2-deoxy-^{14}C]glucose (PerkinElmer) on day 8.0 of pregnancy. After 1 h, mice were sacrificed by cervical dislocation, and individual deciduae, extraembryonic tissues, and embryos were collected separately and lysed overnight in tail lysis buffer (10 mM Tris-Cl, pH 8.0, 100 mM EDTA, pH 8.0, 100 mM NaCl, 1% SDS). Radioisotope uptake was determined from β-emissions of samples placed in scintillation fluid (Starcint; Packard BioScience BV) using a scintillation counter (Tri-Carb 2000; Packard BioScience BV).

Statistical analysis. All statistical analyses were conducted using Stata v9.2 (Statacorp) with one- or two-factor analysis of variance (ANOVA) and Fisher's *post hoc* test. Frequencies of genotypes recovered at various developmental stages were analyzed by chi-square analysis, followed by Fisher's exact test.

RESULTS

***Hbo1* null allele and *Hbo1* mRNA and protein expression.** A conditional *Hbo1* mutant allele was generated as described in Materials and Methods. We used a germ line-expressed cre-recombinase to delete exon 1 of the *Hbo1* gene together with the *neo* selection cassette (Fig. 1A and B). This deletion prevented both the transcription and the translation of the mutant allele. No *Hbo1* mRNA (Fig. 1C to H) or protein (Fig. 1I and J) could be detected in embryonic or extraembryonic tissues in $Hbo1^{-/-}$ embryos. HBO1 protein was present in all cells of the developing $Hbo1^{+/+}$ embryo, and its localization was exclusively nuclear (Fig. 1I). In $Hbo1^{+/+}$ embryos at E8.5 and E9.5, *Hbo1* was expressed ubiquitously in the embryonic and extraembryonic tissues (Fig. 1C to F). High levels of *Hbo1* mRNA were present in the chorionic plate (E8.5 and E9.5) as well as in and around the foregut and hindgut regions (E9.5). *Hbo1* was ubiquitously expressed in all adult tissues examined, with lower levels in the kidney and liver (Fig. 1K). Particularly strong *Hbo1* mRNA expression was detected in testes (Fig. 1K), in common with two other MYST family genes, *Mof* and *Tip60* (66). The observation that *Hbo1* was expressed in the adult brain, a tissue consisting almost exclusively of postmitotic

TABLE 3. ChIP-qPCR primers

Target gene	Primer sequence 5′	Primer sequence 3′	Primer position[a] (bp)	NCBI accession no.
Hoxa3	GCAGCTCTGTCCTCTCCTTG	GCTGTGGTCCTCTCTTGGTC	+1669 (between 4 and 5)	NM_010452.3
Hsp90ab1	AATTGACATCATCCCCAACC	TCGTGCCAGACTTAGCAATG	+360 (at 3)	NM_008302.3
Otx2	TCCCGATGTATTTTCCTTGC	CTTCTGCAGACCCCAGATTC	+199 (between 1 and 2)	NM_144841.3
Tbx1	GCTCCCGATTTGACCAGTAG	GAGAAGGCTTTGCAAACAGG	+923 (between 1 and 2)	NM_011532.1

[a] Position on genomic sequence downstream of ATG. Positions relative to exons are in parentheses.

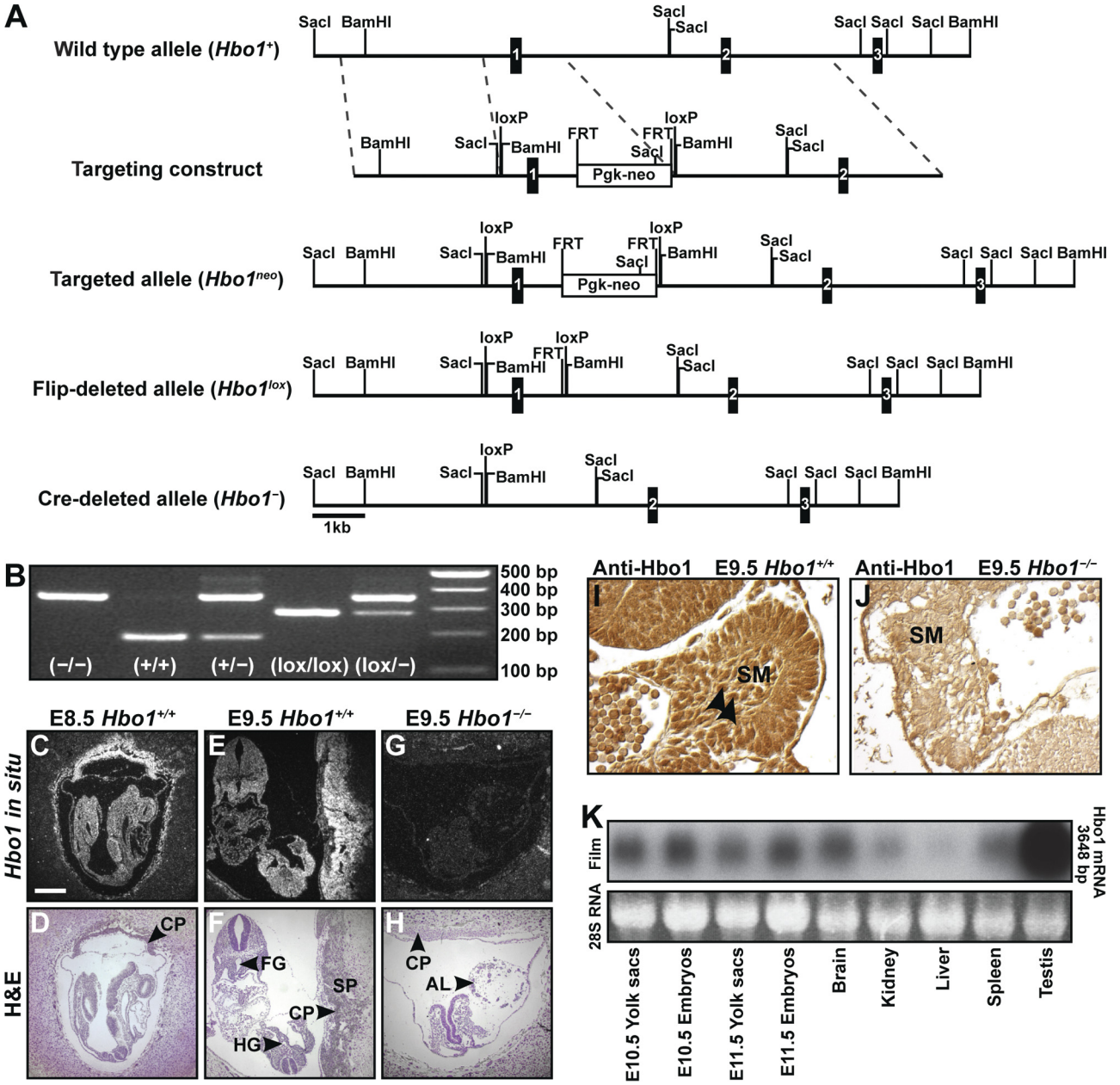

FIG. 1. *Hbo1* mutant alleles and expression patterns. (A) Schematic of wild-type and *Hbo1* mutant alleles, with numbered black boxes representing exons. (B) Three-way PCR used to genotype $Hbo1^{+}$ (wild-type), $Hbo1^{lox}$ (floxed), and $Hbo1^{-}$ (null) alleles, shown here in E8.5 embryos. (C to H) Radioactive RNA *in situ* hybridization depicting strong and ubiquitous *Hbo1* expression at E8.5 and E9.5. Note the particularly high levels of expression in the chorionic plate (CP) at E8.5 and E9.5 as well as in the foregut (FG) and hindgut (HG) regions at E9.5. No *Hbo1* mRNA was detectable in $Hbo1^{-/-}$ embryos (G and H). SP, spongiotrophoblast; AL, allantois; H&E, hematoxylin and eosin. (I and J) HBO1 immunohistochemistry shows strong nuclear localization of HBO1 protein in wild-type controls (arrowheads, I), while no HBO1 protein is present in $Hbo1^{-/-}$ embryos (J). SM, somites. (K) Northern blot showing *Hbo1* mRNA expression in adult and embryonic tissues. Bar, 75 μm (C and D), 350 μm (E and F), 212 μm (G and H), or 162 μm (I and J).

cells, indicated that it is likely that HBO1 possesses cellular functions aside from its proposed role in cell proliferation and DNA replication.

***Hbo1* deletion results in embryonic lethality at E10.5.** Initial germ layer formation and the establishment of the embryonic axes proceeded normally in $Hbo1^{-/-}$ embryos, and no abnormalities were observed prior to E7.5 (E4.5, 15 embryos; E5.5, 19 embryos; E6.5, 32 embryos) (data not shown). At E7.5, $Hbo1^{-/-}$ embryos were within the normal size range seen in wild-type litters (Fig. 2A and B). At E8.0 to E8.5, $Hbo1^{-/-}$ embryos were developmentally delayed by approximately 12 h (Fig. 2C to F), and at E9.5, $Hbo1^{-/-}$ embryos were approximately 24 h developmentally delayed (Fig. 2G and H), in comparison to $Hbo1^{+/+}$ embryos. At this point, $Hbo1^{-/-}$ embryos underwent developmental arrest and did not develop past the 10- to 11-somite stage. As $Hbo1^{-/-}$ embryos featured

a developmental delay, *Hbo1*$^{-/-}$ embryos were stage matched to control embryos by somite count, as indicated in the relevant figure legends and Materials and Methods. At E10.5, *Hbo1*$^{-/-}$ embryos exhibited diminished posterior and midline structures. Nevertheless, 9 out of 18 *Hbo1*$^{-/-}$ embryos had beating hearts at this stage (Fig. 2I and J). No *Hbo1*$^{-/-}$ embryos were recovered at E11.5 ($P = 0.009$) (for numbers of embryos examined, see Table 4), indicating that they underwent resorption shortly after E10.5. In wild-type embryos, the chorion-allantois connection is established between E8.5 and E9.5. In contrast, the allantois of *Hbo1*$^{-/-}$ embryos failed to grow directionally toward the chorionic plate but continued to expand as a highly vascularized, bulbous structure (Fig. 2K and L). *Hbo1*$^{-/-}$ embryos failed to complete axial rotation and developed enlarged blood vessels in the head region at E8.5, which were more prominent at E9.5 (Fig. 2M to P). However, no indication of edema or hemorrhage was observed at any stage. The dorsal aorta and first pharyngeal arch artery were most severely affected, showing grossly dilated lumina, while cells of the surrounding mesenchyme appeared sparse. These vascular defects extended along the entire length of the embryo, where a comparable paucity of mesenchymal cells was evident (Fig. 2Q and R). Similarly, the cardiac inflow tract was dilated in *Hbo1*$^{-/-}$ embryos in comparison to that in control embryos (data not shown). Somites were indistinct and unstructured in E9.5 *Hbo1*$^{-/-}$ embryos (Fig. 2R).

The initial vasculogenic stages of wild-type yolk sac development are marked by the aggregation and fusion of blood island endothelial cells to form the primitive capillary plexus, a structure composed of a polygonal network of immature vessels, at E8. At E9, the vascular plexus undergoes extensive angiogenic remodeling to give rise to a hierarchical array of small- and large-caliber vessels (50). Highly disorganized *Hbo1*$^{-/-}$ yolk sac vascular branching and patterning were revealed by anti-CD31 (PECAM) immunofluorescence staining (Fig. 2S to V; 6 *Hbo1*$^{-/-}$ and 8 *Hbo1*$^{+/+}$ embryos). At E8.5, blood vessels in *Hbo1*$^{-/-}$ yolk sacs were disordered, forming thin networks with the presence of abnormal endothelial cell clusters. These networks appeared to fuse randomly and remained undeveloped at E9.5, where large vitelline vessels failed to form and the vascular plexus persisted in a primitive state (Fig. 2S to V).

***Hbo1*$^{-/-}$ embryos display adequate vascular and placental function.** As we observed defects in vascular and placental morphology, we examined whether parameters of vascular and placental function were normal in *Hbo1*$^{-/-}$ embryos. Nidogen is important in stabilizing basement membranes and is particularly strongly expressed in vascular endothelial cells (65), where it may also have a role in regulating angiogenesis (45). Nidogen distribution was found to be normal in *Hbo1*$^{-/-}$ embryos and expressed at a level similar to that for *Hbo1*$^{+/+}$ controls (data not shown); together with no obvious observation of hemorrhage or edema, our data show that the mechanical integrity of vessel walls remained intact in *Hbo1*$^{-/-}$ embryos.

To investigate the functional consequences of yolk sac vascular abnormalities and the failure of chorioallantoic fusion in *Hbo1*$^{-/-}$ embryos, we conducted transplacental nutrient uptake assays and measured levels of hypoxia to assess if these factors contributed to the restriction in developmental progression in these embryos. Dams were injected with radiolabeled [^{14}C]glucose at E8.0, at which point chorioallantoic fusion had not occurred in *Hbo1*$^{-/-}$ or control embryos. We observed no significant differences among *Hbo1*$^{+/+}$, *Hbo1*$^{+/-}$, and *Hbo1*$^{-/-}$ tissues in radioisotope uptake (data not shown), ruling out the possibility of glucose deficiency being the limiting factor for normal developmental progression in *Hbo1*$^{-/-}$ embryos, at least prior to E8.0. HIF-1α is a transcription factor that is strongly upregulated under hypoxic conditions (25) and that promotes vascular development by stabilizing vascular endothelial growth factor (VEGF) (38). However, the absence of HIF-1α staining in E8.5 and E9.5 *Hbo1*$^{-/-}$ embryos (data not shown) suggested that hypoxia did not contribute to the *Hbo1*$^{-/-}$ phenotype.

***Hbo1*$^{-/-}$ cells are not deficient in proliferation or DNA replication.** HBO1 has previously been reported to be required for DNA replication and cell proliferation. To determine if intrinsic defects in proliferation contributed to *Hbo1*$^{-/-}$ growth retardation and eventual developmental arrest, we conducted a series of *in vivo* and *in vitro* assays.

We cultured E3.5 blastocysts and examined these for a period of 7 days to assess proliferation and differentiation. No discernible differences were observed throughout the culture period; all blastocysts hatched from the zona pellucida, attached, and proliferated to form the two expected cell types, the inner cell mass outgrowths and the surrounding trophoblasts (Fig. 3A and B; 5 *Hbo1*$^{-/-}$, 25 *Hbo1*$^{+/-}$, and 11 *Hbo1*$^{+/+}$ embryos).

We cultured dissociated E9.5 embryos in fibroblast enriching medium and found that morphologically normal primary embryonic fibroblasts (PEFs) could be derived from *Hbo1*$^{-/-}$ embryos (Fig. 3C and D). MTT cell proliferation assays showed robust proliferation of PEFs of all three genotypes and no differences in proliferation rate between control and *Hbo1*$^{-/-}$ PEFs throughout all 5 days of culture (Fig. 3E; $P = 0.9997$; PEF isolates from 5 *Hbo1*$^{-/-}$, 5 *Hbo1*$^{+/-}$, and 5 *Hbo1*$^{+/+}$ embryos). Furthermore, cell cycle analyses revealed that there were no differences in overall distribution of cells in the G_0/G_1 ($P = 0.302$), S ($P = 0.621$), and G_2/M ($P = 0.245$) phases of the cell cycle within *Hbo1*$^{-/-}$ and *Hbo1*$^{+/+}$ PEF cultures (Fig. 3F; PEF isolates from 3 *Hbo1*$^{-/-}$ and 3 *Hbo1*$^{+/+}$ embryos).

Hbo1$^{lox/lox}$ fibroblast lines, either positive or negative for a *Cre-ERT* transgene, were treated with tamoxifen for 24 h and passaged in culture for 15 weeks in the absence of tamoxifen. This allowed the study of the effects of an acute as well as a long-term loss of HBO1. We did not observe changes in cell morphology or excessive cell death in *Hbo1*$^{lox/lox}$ *Cre*$^{T/+}$ cell lines in comparison to results for *Hbo1*$^{lox/lox}$ *Cre*$^{+/+}$ control cell lines following tamoxifen treatment. Tamoxifen-induced cre deletion during the initial 24 h was not 100% efficient in all cultures and so gave rise to a mixture of *Hbo1* undeleted (*Hbo1*$^{lox/lox}$ *Cre*$^{T/+}$), partially deleted (*Hbo1*$^{lox/-}$ *Cre*$^{T/+}$), and completely deleted (*Hbo1*$^{-/-}$ *Cre*$^{T/+}$) cultures. This created a competitive environment within some cultures, in which selective pressure against fibroblast genotypes that have subtle defects in proliferation could be observed. After 3 days of culture, no recombination was observed in *Hbo1*$^{lox/lox}$ *Cre*$^{+/+}$ control cell lines, as expected, whereas a high degree of recombination was seen in *Hbo1*$^{lox/lox}$ *Cre*$^{T/+}$ cell lines (Fig. 3G; each lane

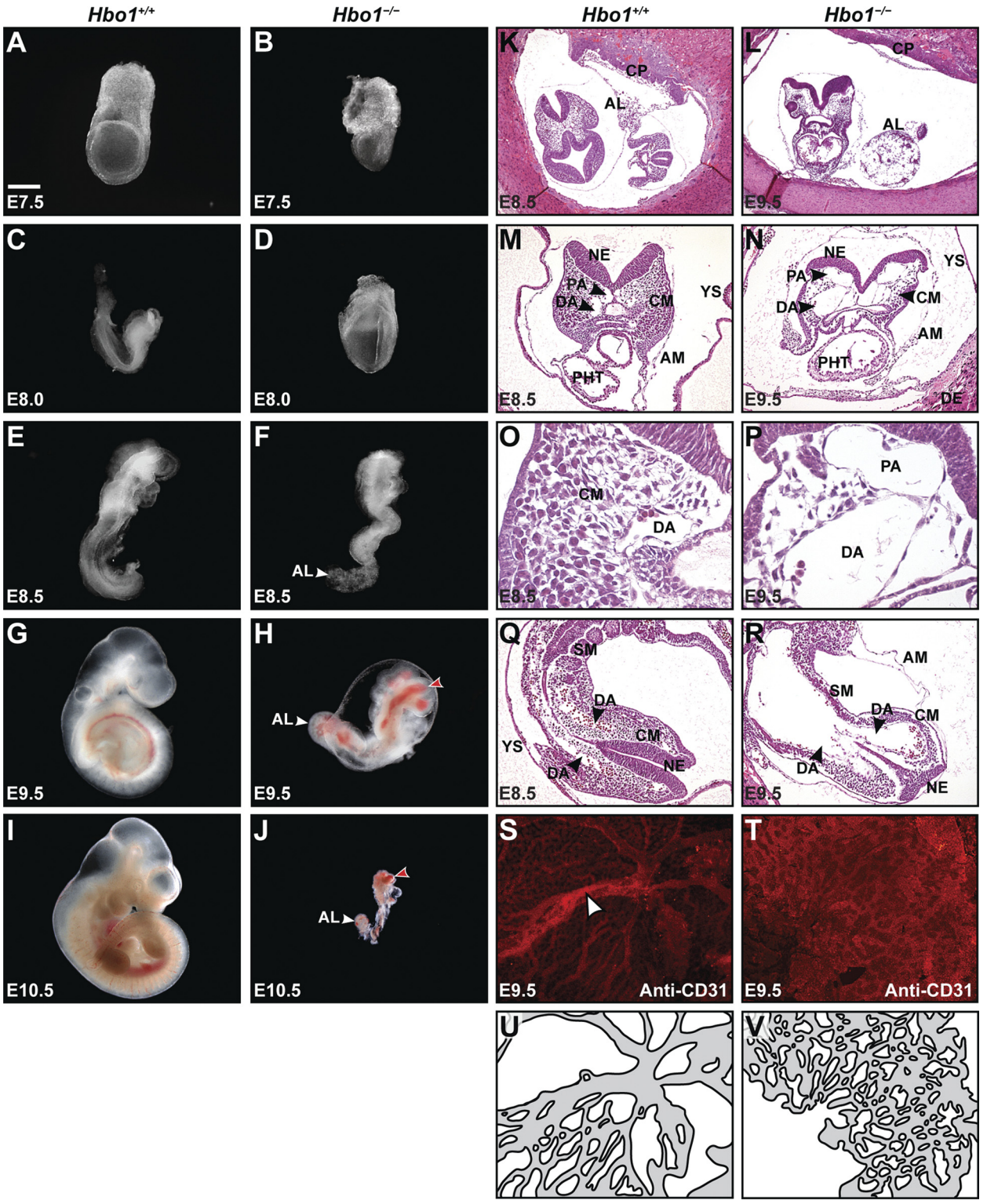

FIG. 2. Gross morphology and histology of *Hbo1*$^{-/-}$ embryos. (A to J) Eight of 12 *Hbo1*$^{-/-}$ embryos are small albeit still within the size range seen in wild-type E7.5 litters (A and B) but become progressively growth retarded in comparison to age-matched *Hbo1*$^{+/+}$ controls as development proceeds. Note the bulbous shape of the allantois (white arrowheads, F, H, and J) and the large blood sinuses (red arrowheads, H and J) and the failure of axial rotation in *Hbo1*$^{-/-}$ embryos. (K to R) Hematoxylin- and eosin-stained sections of E9.5 *Hbo1*$^{-/-}$ embryos and stage-matched E8.5 *Hbo1*$^{+/+}$ controls. Note the failure of chorioallantoic fusion (K and L), expanded dorsal aorta and first pharyngeal arch arteries (M to R), and reduction of cephalic mesenchyme- and mesoderm-derived structures, such as somites (Q and R), in *Hbo1*$^{-/-}$ embryos. (S to V) Whole-mount anti-CD31 (PECAM) staining of yolk sacs (S and T) and corresponding traces of blood vessels (U and V). Note the absence of large vitelline vessels in *Hbo1*$^{-/-}$ mutants (arrowhead, S). AL, allantois; AM, amnion; CM, cephalic mesenchyme; CP, chorionic plate; DA, dorsal aorta; DE, decidua; NE, neural ectoderm; PA, first pharyngeal arch artery; PHT, primitive heart tube; SM, somite; YS, yolk sac. Bar, 86 μm (A to D), 142 μm (E and F), 245 μm (G and H), 730 μm (I and J), 160 μm (K and L), 80 μm (M and N), 201 μm (O and P), 80 μm (Q and R), or 68 μm (S to V).

TABLE 4. Distribution of the *Hbo1*$^{-}$ allele among offspring of *Hbo1*$^{+/-}$ intercrosses

Developmental stage	No. (%) of embryos of *Hbo1*$^{+/-}$ intercrosses			Total no. of embryos
	Hbo1$^{+/+}$	*Hbo1*$^{+/-}$	*Hbo1*$^{-/-}$	
E7.5	12 (26)	22 (48)	12 (26)	46
E8.5	30 (26)	54 (47)	31 (27)	115
E9.5	23 (26)	48 (53)	19 (21)	90
E10.5	26 (30)	44 (50)	18 (20)[a]	88
E11.5	10 (33)	20 (67)	0 (0)[b]	30

[a] Nine of 18 *Hbo1*$^{-/-}$ embryos had beating hearts at E10.5.
[b] All *Hbo1*$^{-/-}$ embryos examined prior to E10.5 had beating hearts (P = 0.009).

represents an independent cell line isolated from one embryo). Notably, cell line 11 consisted purely of *Hbo1*$^{-/-}$ *Cre*$^{T/+}$ cells after 3 days of culture, continued proliferating normally, and remained viable 15 weeks later (Fig. 3H). We observed detectable levels of undeleted *Hbo1* alleles in cell line 7 after 3 days of culture. However, by 15 weeks, cell line 7 consisted purely of *Hbo1* $^{-/-}$ *Cre*$^{T/+}$ cells. In the case of cell line 9, the relative proportions of deleted and undeleted alleles remained similar over the 15 weeks of analysis. These results show that *Hbo1*$^{-/-}$ *Cre*$^{T/+}$ cells were capable of continuous long-term proliferation and that *Hbo1*$^{-/-}$ *Cre*$^{T/+}$ cells were not outcompeted by *Hbo1*$^{lox/lox}$ *Cre*$^{T/+}$ or *Hbo1*$^{lox/-}$ *Cre*$^{T/+}$ cells.

Importantly, BrdU incorporation experiments revealed that there was no significant difference (P = 0.827) in the percentages of cell nuclei undergoing DNA synthesis in E8.0 *Hbo1*$^{+/+}$ control embryos (Fig. 3I; 66% ± 2.9%; 9 embryos) and E8.5 *Hbo1*$^{-/-}$ embryos (Fig. 3J; 65% ± 5.5%; 3 embryos). All tissues in the developing *Hbo1*$^{-/-}$ embryo showed a high level of BrdU staining, and *Hbo1*$^{-/-}$ cells exhibited staining intensities similar to those of wild-type control cells, indicating that *Hbo1*$^{-/-}$ embryos were as effective as wild-type controls in incorporating BrdU into newly synthesized DNA and that DNA replication ensued at normal rates in *Hbo1*$^{-/-}$ embryos.

We examined the cellular localization of MCM2 in *Hbo1*$^{-/-}$ embryos compared to that in *Hbo1*$^{+/+}$ embryos. The MCM2 to -7 complex exhibits DNA helicase activity and is essential in separating the DNA double helix into single strands to facilitate DNA replication (5). Within this complex, MCM2 has been demonstrated to interact with HBO1 (9), and the knockdown of HBO1 using RNAi in HeLa cells has been reported to result in a shift in localization of MCM2 protein from a nuclear to a cytoplasmic cellular fraction (26). In contrast, we found that MCM2 staining was present at normal levels and was predominantly nuclear in *Hbo1*$^{-/-}$ embryos, as it was in *Hbo1*$^{+/+}$ embryos, indicating that a loss of HBO1 had no influence on MCM2 localization (Fig. 3K and L; 8 *Hbo1*$^{-/-}$ and 13 control embryos).

We found that the lack of HBO1 affected cell survival rather than DNA replication. TUNEL staining revealed an 8-fold increase in the percentage of cells undergoing cell death in *Hbo1*$^{-/-}$ embryos, resulting in a 3-fold reduction in the number of cells per section (Fig. 3M and N; $P < 0.0001$ and P = 0.0304, respectively; 3 *Hbo1*$^{-/-}$, 6 *Hbo1*$^{+/-}$, and 3 *Hbo1*$^{+/+}$ E8.5 to E9.5 embryos). Collectively, with respect to the *Hbo1*$^{-/-}$ phenotype, our data suggest that the reduction in embryo size and cell number is primarily due to cell death, rather than deficiencies in cell proliferation.

HBO1 is an essential regulator of gene expression. To determine if the lack of HBO1 affected the expression of key regulatory genes involved in patterning the early embryo, we examined the expression profiles of 17 genes in a total of 102 embryos (3 *Hbo1*$^{-/-}$ and 3 *Hbo1*$^{+/+}$ embryos per probe) by whole-mount *in situ* hybridization (WMISH).

We characterized the expression of essential regulators of heart development *Nkx2.5*, *Gata4*, and *Tbx1* (59). While the hearts of *Hbo1*$^{-/-}$ embryos appeared morphologically normal, apart from a modest dilation of the inflow tracks, and continued to beat until E9.5 to E10.5, cardiac patterning genes *Nkx2.5*, *Gata4*, and *Tbx1* were found to be underexpressed in *Hbo1*$^{-/-}$ hearts. Interestingly, the expression of primary heart field regulators *Nkx2.5* and *Gata4* was detectable in the cardiac inflow tracts but was markedly reduced in the heart chambers of *Hbo1*$^{-/-}$ embryos (Fig. 4A to D). *Tbx1* is expressed strongly in the pharyngeal endoderm and is important for inducing the specification of the cardiac outflow tract in the underlying pharyngeal mesoderm. *Tbx1* expression was reduced in *Hbo1*$^{-/-}$ embryos (Fig. 4E and F).

As we observed abnormal vascular development in *Hbo1*$^{-/-}$ embryos, we investigated the expression of genes involved in blood vessel development. Key regulators of vascular development include *VegfA*, *Flk-1*, *Tie-1*, and *Tie-2* (50). Although *VegfA* expression appeared unchanged in *Hbo1*$^{-/-}$ embryos (Fig. 4G and H), the expression of its receptor, *Flk-1*, was reduced in *Hbo1*$^{-/-}$ embryos but remained strong in the allantois (Fig. 4I and J). Similarly, the expression of angiopoietin receptors *Tie-1* and *Tie-2* was also downregulated, particularly in regions outside the cardiac inflow tract, in *Hbo1*$^{-/-}$ embryos, whereas the expression of *Tie-1* remained strong in the allantois (Fig. 4K to N).

Flk-1 knockout embryos die between E8.5 and E9.5 due to defects in hematopoietic and endothelial cell development, where yolk sac blood islands were absent and the dorsal aorta was greatly reduced in diameter (56). *Tie-1* knockout embryos die between E13.5 and E14.5 due to severe edema and vascular hemorrhaging (48), whereas *Tie-2* knockout embryos die at E10.5 due to endocardial defects, hemorrhaging, significant reductions in endothelial cells, and collapsed vasculature (15). Even though *Flk-1*, *Tie-1*, and *Tie-2* expression was substantially downregulated in *Hbo1*$^{-/-}$ embryos, there was no evidence of hemorrhaging, heart defects, blood island abnormalities, or reductions in the size of the vascular lumen. Rather, the vascular lumina are grossly expanded in *Hbo1*$^{-/-}$ embryos at E9.5. This suggests a failure of the vasculature to progress from an immature and primitive state to the angiogenic remodeling stage.

The level of *Hex* mRNA, an early marker of endothelial precursors (62), was modestly reduced in the head region of *Hbo1*$^{-/-}$ embryos (Fig. 4O and P). The Ets transcription factor *Erg*, which is essential for hematopoiesis in mice (40), is also expressed in the vasculature (Fig. 4Q) and was significantly reduced in the *Hbo1*$^{-/-}$ embryo proper but was present in the allantois at normal levels (Fig. 4R).

The *Drosophila* homologue of HBO1, chameau, has been demonstrated to promote heterochromatin-mediated gene silencing and to act as a silencer of bithorax group homeotic

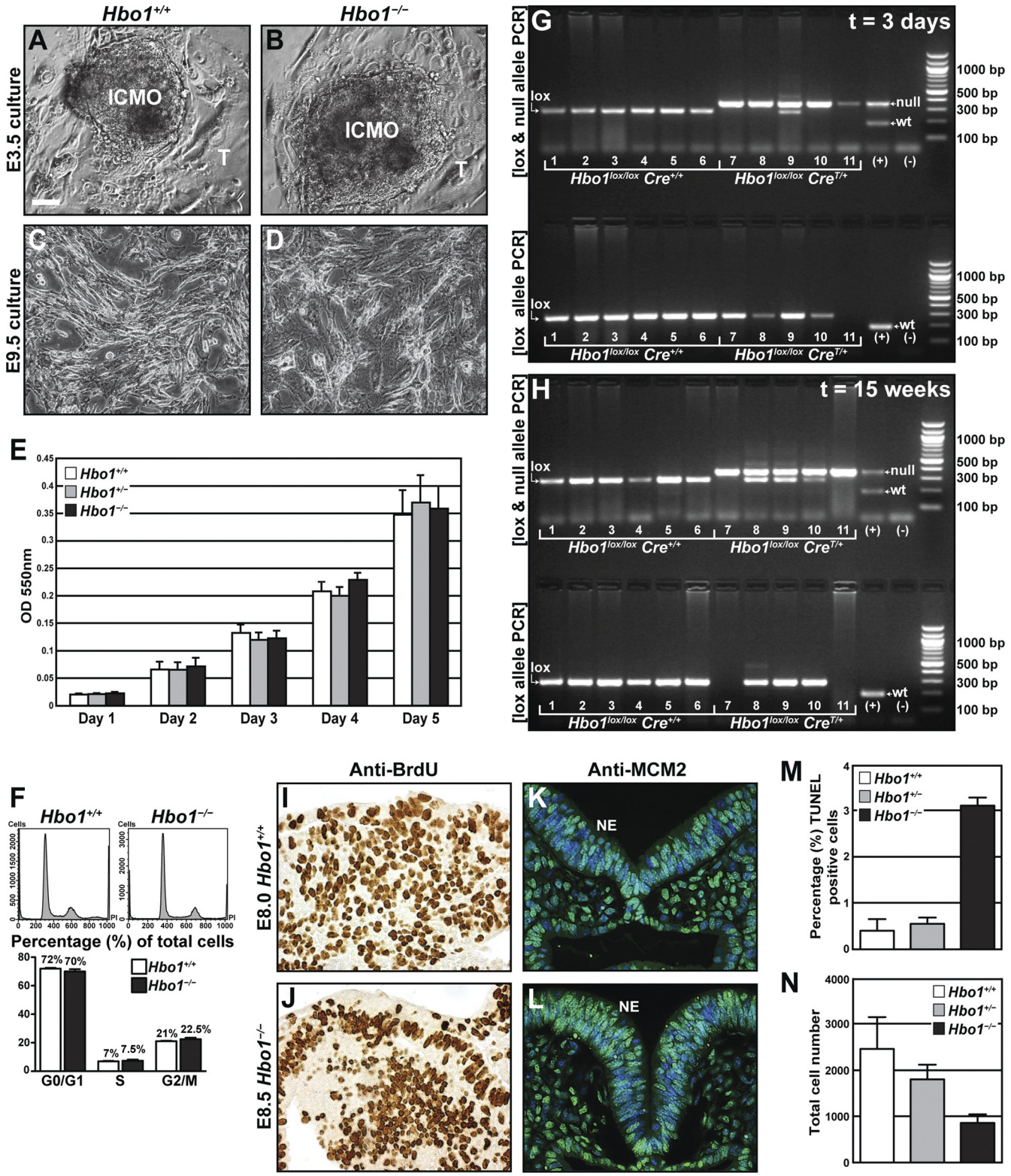

FIG. 3. Cell proliferation and DNA replication proceeded normally in the absence of HBO1. (A and B) *Hbo1*$^{-/-}$ and *Hbo1*$^{+/+}$ E3.5 cultures proliferated and formed normal inner cell mass outgrowths (ICMO) and surrounding trophoblasts (T) by day 7 of culture. (C and D) Normal primary embryonic fibroblasts could be derived from E9.5 *Hbo1*$^{-/-}$ and *Hbo1*$^{+/+}$ embryos. (E) Results from MTT proliferation assay, showing no difference in proliferation between fibroblasts derived from *Hbo1*$^{+/+}$ and *Hbo1*$^{-/-}$ embryos ($P = 0.9997$). OD, optical density. (F) FACS histogram of propidium iodide (PI)-stained *Hbo1*$^{-/-}$ and *Hbo1*$^{+/+}$ PEFs, showing no significant differences in distribution of cells within G_0/G_1 ($P = 0.302$), S ($P = 0.621$), and G_2/M ($P = 0.245$) phases of the cell cycle. (G) PCR amplification of DNA extracted from long-term *Hbo1*$^{lox/lox}$ *Cre*$^{+/+}$ fibroblast lines (lanes 1 to 6) and *Hbo1*$^{lox/lox}$ *Cre*$^{T/+}$ cell lines (lanes 7 to 11) (isolated from one embryo each) on day 3 after tamoxifen treatment. As expected,

gene expression by genetically interacting with polycomb group proteins (20). Based on this, we expected to see overexpression of *Hox* genes in *Hbo1*$^{-/-}$ mouse embryos. However, unexpectedly, and in contrast to the effects of a loss of chameau in *Drosophila*, *Hoxa2* expression was significantly reduced in *Hbo1*$^{-/-}$ embryos, while *Hoxa3* staining appeared at an intensity similar to that in wild-type controls (Fig. 5A to D). *Otx2* (6) and *Sox2* (52) are essential genes required for patterning the neural ectoderm. Both *Otx2* and *Sox2* were expressed at reduced levels in *Hbo1*$^{-/-}$ embryos postgastrulation (Fig. 5E to H). During normal development, *Otx2* is expressed throughout the epiblast and also in the visceral endoderm. However, *Otx2* has a dynamic pattern of expression, and as development proceeds, its expression becomes progressively restricted to the head region (1). Interestingly, we found that *Otx2* expression in *Hbo1*$^{-/-}$ embryos was normal at the onset of gastrulation in the epiblast (data not shown), suggesting that HBO1 is necessary for the maintenance of *Otx2* expression in newly patterned tissue domains.

brachyury (58), *Shh* (12), and *Notch1* (19) are important regulatory genes expressed during gastrulation. We observed that *Notch1* expression was low in most areas of the paraxial and presomitic mesoderm in *Hbo1*$^{-/-}$ embryos (Fig. 5I and J). Limited areas of normal expression gave the *Notch1* expression pattern a variegated appearance in the presomitic mesoderm of *Hbo1*$^{-/-}$ embryos, whereas no *Notch1* expression was detected in the somitic region of *Hbo1*$^{-/-}$ embryos. On the other hand, the floorplate and notochord marker *Shh* and the essential regulator of mesoderm development *brachyury* were expressed at relatively normal levels in *Hbo1*$^{-/-}$ embryos in comparison to wild-type controls as assessed by WMISH (Fig. 5K to N). In addition, similar expression levels of the constitutively expressed chaperone *Hsp90ab1* (*Hsp90*β [72]) in *Hbo1*$^{+/+}$ and *Hbo1*$^{-/-}$ embryos (Fig. 5O and P) further confirmed that the reduction in expression of multiple genes seen in *Hbo1*$^{-/-}$ embryos was not simply an inevitable consequence of tissue degeneration and cell death.

Overall, there was a significant reduction in expression of the majority of genes examined in *Hbo1*$^{-/-}$ embryos, and in no case was an increase in gene expression observed in *Hbo1*$^{-/-}$ embryos, indicating that HBO1 functions as a general activator of gene expression.

H3K14 acetylation displays a nonredundant requirement for HBO1. To identify specific histone residues acetylated by HBO1, we examined differences in histone acetylation patterns between *Hbo1*$^{+/+}$ and *Hbo1*$^{-/-}$ PEFs isolated from E9.5 embryos. *Hbo1*$^{-/-}$ PEFs had more than a 10-fold reduction in H3K14 acetylation (Fig. 6A and B; $P < 0.0001$; 3 independent PEF isolates from 3 embryos per genotype, with one PEF isolate per lane). Interestingly, there was a significant 3-fold increase in H4K16 acetylation ($P = 0.0098$) in *Hbo1*$^{-/-}$ cells. In addition, H3K9 ($P = 0.0029$) and H4K5 ($P = 0.024$) acetylation levels were significantly increased, 46% and 20%, respectively, while H4K8 and H4K12 acetylation levels were largely unchanged, in *Hbo1*$^{-/-}$ cells.

We considered the possibility that HBO1 could directly regulate other histone acetyltransferases at the transcriptional level and that the deregulation of these histone acetyltransferases, as a consequence of a loss of HBO1, could account for the observed changes in histone acetylation patterns. Thus, we assessed the expression of essential histone acetyltransferases in *Hbo1*$^{-/-}$ PEFs by RT-qPCR, normalizing against *Pgk1*, *Rpl13a*, *Hsp90ab1*, *Psmb2*, and *B-actin*. We found a 37% increase in *Mof* transcripts in *Hbo1*$^{-/-}$ PEFs ($P = 0.016$), whereas *Moz* ($P = 0.970$) and *Gcn5* ($P = 0.930$) expression levels were not significantly changed (Fig. 6C; 3 independent PEF isolates from 3 embryos per genotype). In addition, there were no changes in GCN5 (KAT2A) protein levels in *Hbo1*$^{-/-}$ PEFs (Fig. 6D and E; $P = 0.426$; 3 independent PEF isolates from 3 embryos per genotype).

***Hbo1*$^{-/-}$ embryos feature reduced H3K14 acetylation at gene coding regions and a general depression of transcriptional activity.** To quantify gene expression levels in *Hbo1*$^{-/-}$ embryos at E8.5 and E9.5, we conducted a series of RT-qPCR experiments (Fig. 7A to D). The expression levels of a range of regulatory genes were then determined relative to those of the housekeeping genes *Hsp90ab1*, *Pgk1*, and *Rpl13a*. We observed that the amount of total RNA isolated per embryo at E9.5 was 2-fold lower in the *Hbo1*$^{-/-}$ embryos than in the controls (2.1 ± 0.2 versus 4.0 ± 0.6 μg/embryo; 5 *Hbo1*$^{-/-}$ and 5 stage-matched wild-type embryos; $P = 0.019$). This discrepancy was observed despite that fact that the *Hbo1*$^{-/-}$ embryos were similar in size to the control embryos, although, as described above, mutant embryos display a lack of mesenchyme. Nevertheless, this reduction in total RNA in *Hbo1*$^{-/-}$ embryos is consistent with a global effect of HBO1 on the level of gene transcription. For subsequent cDNA synthesis, equal amounts of RNA from *Hbo1*$^{-/-}$ and stage-matched wild-type control embryos were used, and qPCR results were normalized to levels for housekeeping genes. Therefore, the large difference observed in the initial amounts of total RNA was not represented in the RT-qPCR results, and this needs to be taken into consideration when comparing WMISH and RT-qPCR results.

At E8.5, we observed significant reductions in expression of

only *Hbo1*$^{lox/lox}$ *Cre*$^{T/+}$ cells displayed cre deletion and the presence of the *Hbo1*$^{-}$ (null) band, whereas *Hbo1*$^{lox/lox}$ *Cre*$^{+/+}$ cells remained undeleted, with the presence of only the *Hbo1*^{lox} (lox) band. Top lanes represent DNA samples amplified for the *Hbo1*^{lox} and *Hbo1*$^{-}$ allele concurrently, while bottom lanes represent the same samples amplified for the *Hbo1*^{lox} allele alone. Note that sample 11 showed the presence of the *Hbo1*$^{-}$ allele but not the *Hbo1*^{lox} allele, which indicates the presence of a pure population of *Hbo1*$^{-/-}$ cells. (H) PCR amplification of DNA extracted from the same samples 15 weeks and 15 passages later. Sample 11 was still proliferating normally and remained comprised entirely of deleted cells. In addition, sample 7 consisted purely of *Hbo1*$^{-/-}$ cells at this stage. (+), *Hbo1*$^{+/-}$ positive DNA control; (−), no-DNA negative control; wt, wild-type band. (I and J) BrdU immunohistochemistry, showing similar levels of BrdU incorporation in stage-matched *Hbo1*$^{+/+}$ and *Hbo1*$^{-/-}$ embryos. (K and L) MCM2 immunofluorescence counterstained with bisbenzimide, showing similar levels and nuclear localization of MCM2 in stage-matched *Hbo1*$^{+/+}$ and *Hbo1*$^{-/-}$ embryos. NE, neural ectoderm. (M) Percentages of TUNEL-positive cells undergoing cell death. (N) Total cell number per section. Data are presented as means ± standard errors of the means (SEM) and were analyzed as described in Materials and Methods. Bar, 94 μm (A to D) or 46 μm (I to L).

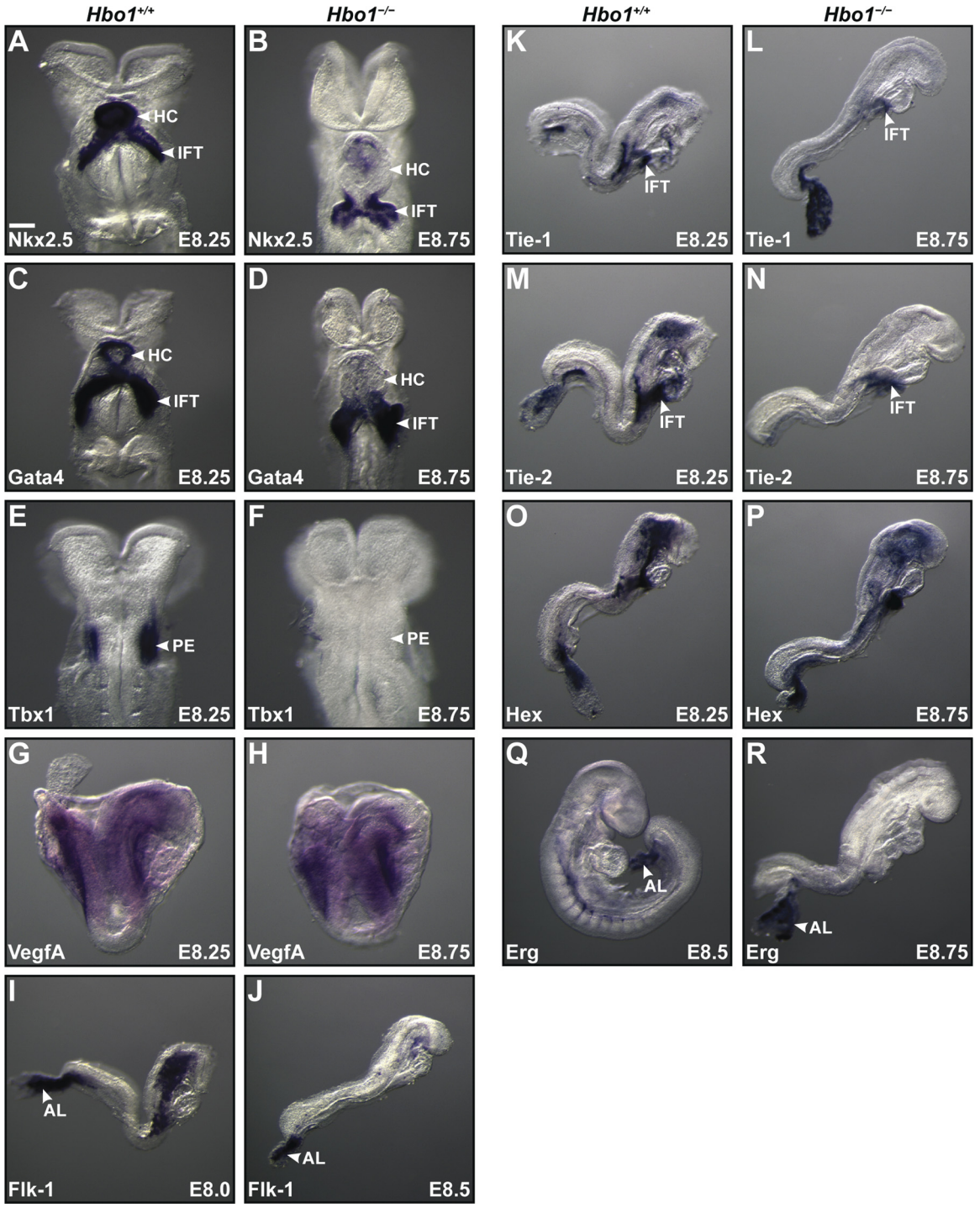

FIG. 4. Whole-mount RNA *in situ* hybridization detecting mRNA (purple staining) of *Nkx2.5*, *Gata4*, *Tbx1*, *VegfA*, *Flk-1*, *Tie-1*, *Tie-2*, *Hex*, and *Erg* in stage-matched $Hbo1^{+/+}$ and $Hbo1^{-/-}$ embryos. Note the reduced expression of most genes, whereas *VegfA* expression was less affected, in $Hbo1^{-/-}$ embryos. AL, allantois; HC, heart chamber; IFT, inflow track; PE, pharyngeal endoderm. Bar, 70 μm (A and B), 130 μm (C and D), 70 μm (E and F), or 185 μm (G to R).

brachyury in $Hbo1^{-/-}$ embryos (Fig. 7A). While the mean expression levels of other genes were lower, the differences were not statistically significant. At E9.5, expression of *brachyury*, *Sox1*, *Sox2*, *Hoxa3*, and *Tie-2* was significantly reduced, while the mean expression levels of other genes were reduced but not significantly so (Fig. 7B and C). In addition, the expression of genes encoding histone acetyltransferases, *Moz*, *Gcn5*, and *Mof*, was significantly reduced in $Hbo1^{-/-}$ embryos (Fig. 7D).

These results show that, relative to those of housekeeping

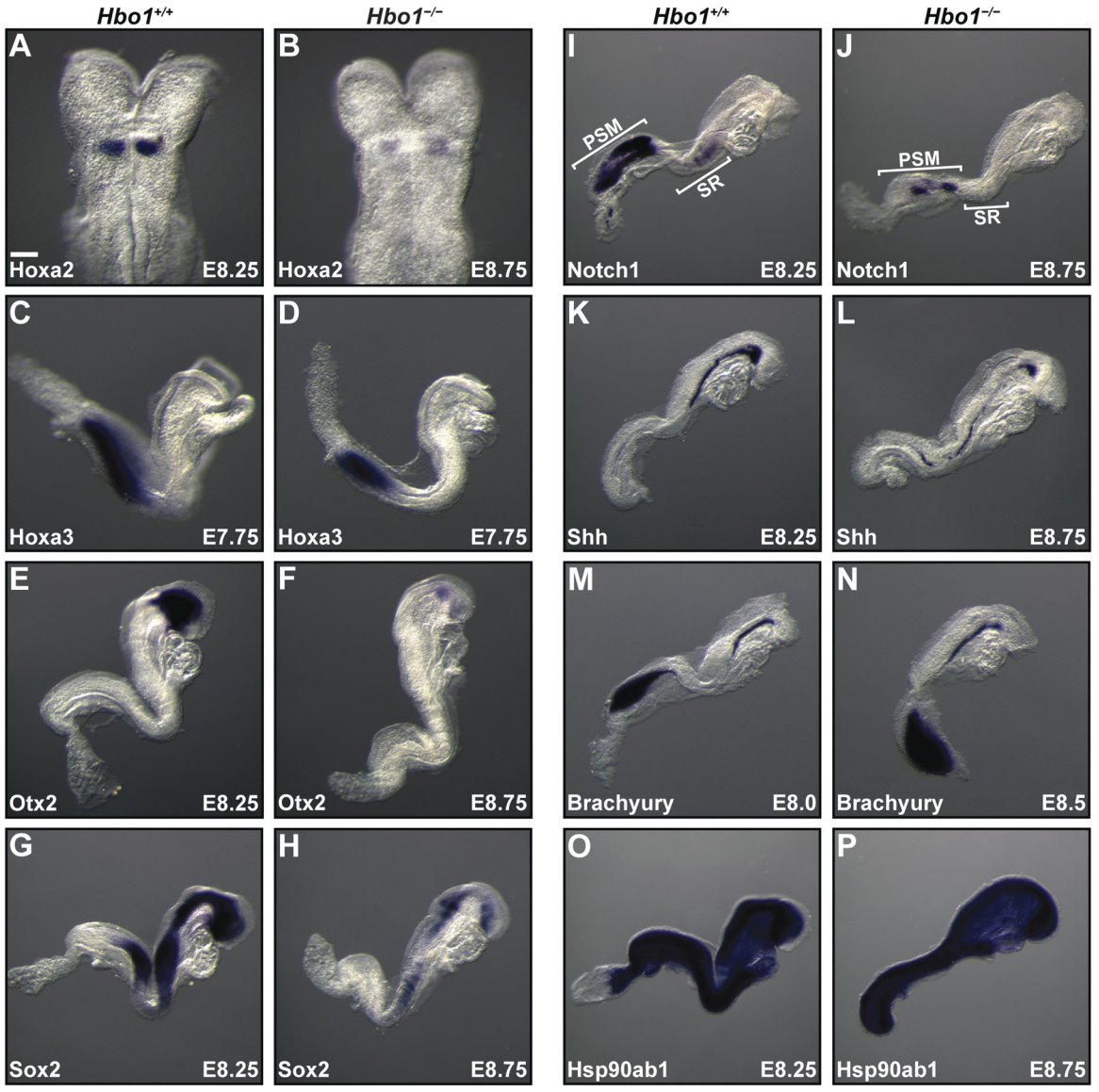

FIG. 5. Whole-mount RNA *in situ* hybridization detecting mRNA (purple staining) of *Hoxa2*, *Hoxa3*, *Otx2*, *Sox2*, *Notch1*, *Shh*, *brachyury*, and *Hsp90ab1* in stage-matched $Hbo1^{+/+}$ and $Hbo1^{-/-}$ embryos. Note the reduced expression of most genes, whereas *brachyury* and *Hsp90ab1* expression was less affected, in $Hbo1^{-/-}$ embryos. PSM, presomitic mesoderm; SR, somite region. Bar, 70 μm (A and B), 135 μm (C and D), or 185 μm (E to P).

genes, the expression levels of the majority of genes patterning the postgastrulation embryo show a decrease, as seen in our WMISH experiments. Importantly, using RT-qPCR or WMISH, we did not detect significant increases in expression of any of the genes analyzed. This indicates that, at least for these particular loci, HBO1 functions as a transcriptional activator rather than having a previously reported role in transcriptional repression (11, 20, 57).

Chromatin immunoprecipitation-quantitative PCR (ChIP-qPCR) experiments using an anti-acetylated H3K14 antibody revealed significant decreases in H3K14 acetylation in the coding regions of *Hoxa3* (58% decrease; $P < 0.001$), *Tbx1* (50% decrease; $P < 0.001$), and *Otx2* (53% decrease; $P < 0.001$) in chromatin material derived from E8.5 $Hbo1^{-/-}$ embryos (Fig. 7E; 6 $Hbo1^{-/-}$ and 6 $Hbo1^{+/+}$ embryos). Significant reductions in acetylation were observed for *Hoxa3* (46% decrease; $P < 0.001$), *Tbx1* (37% decrease; $P = 0.002$), and *Otx2* (42% decrease; $P < 0.001$) even after normalization to acetylation levels at the *Hsp90ab1* locus (Fig. 7F).

DISCUSSION

In this study, we have shown that HBO1 is an essential activator of patterning genes required for the normal development of postgastrulation embryos. Our data suggest that H3K14 is the primary target of HBO1 acetyltransferase activity. Contrary to previously published *in vitro* observations, we found that HBO1 is not essential for cell proliferation or DNA replication *in vivo* or *in vitro*.

As HBO1 has been implicated in DNA replication (26, 32, 44), we expected a peri-implantation lethal phenotype of $Hbo1^{-/-}$ embryos at or prior to E4.5, since our previous work

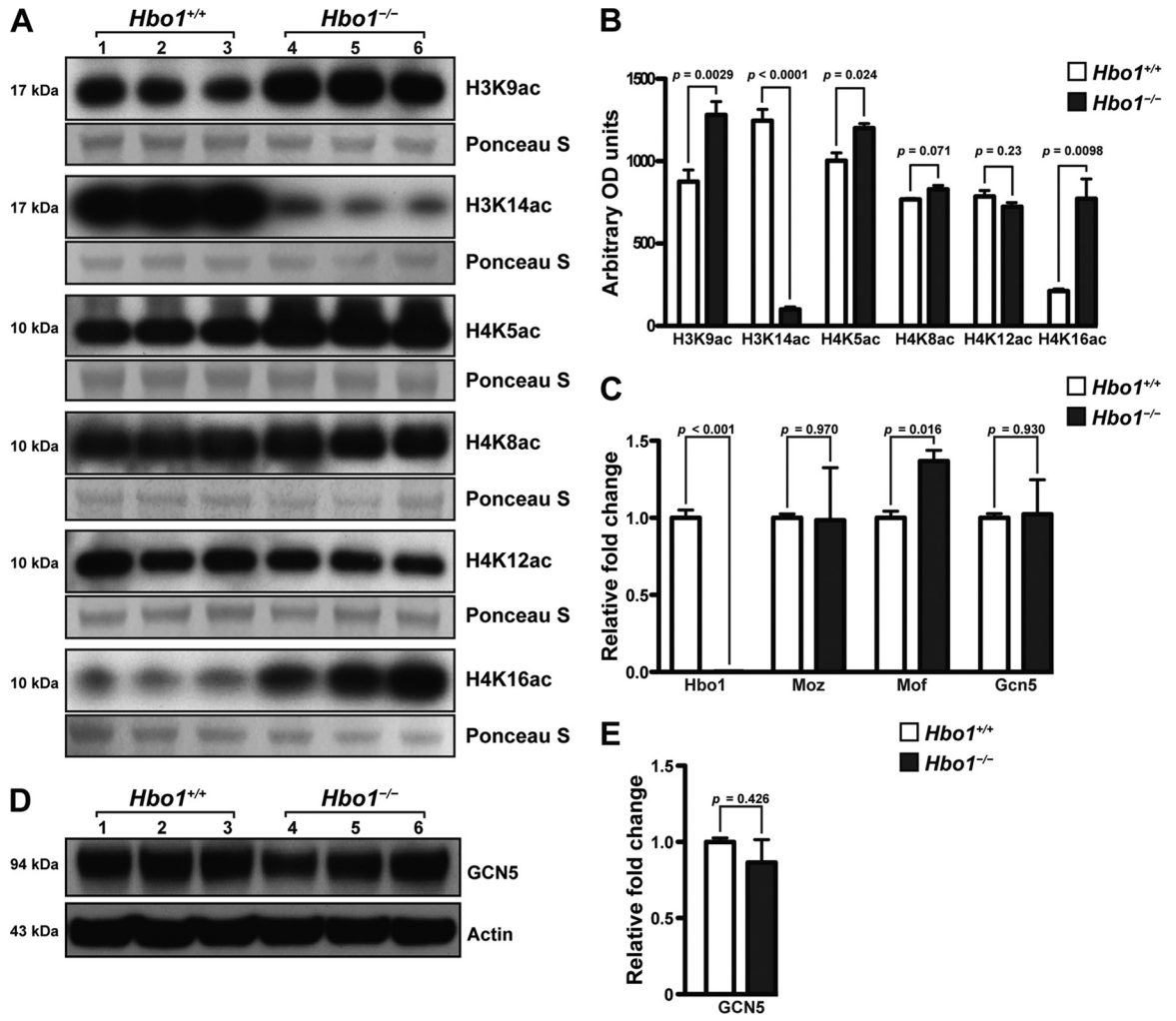

FIG. 6. Acetylation status analysis of H3 and H4 lysine residues in *Hbo1*$^{+/+}$ and *Hbo1*$^{-/-}$ PEFs. (A) Western blots of total PEF lysate probed for acetylated H3K9, H3K14, H4K5, H4K8, H4K12, and H4K16 residues. Blots were stained with Ponceau S as a loading control. (B) Mean densitometry readings of exposed film. Note the significant decrease in H3K14 acetylation (H3K14ac) ($P < 0.0001$), whereas H3K9ac ($P = 0.0029$), H4K5ac ($P = 0.024$), and H4K16ac ($P = 0.0098$) were significantly increased, in *Hbo1*$^{-/-}$ cells. There were no significant differences in H4K8ac ($P = 0.071$) and H4K12ac ($P = 0.23$) between *Hbo1*$^{+/+}$ and *Hbo1*$^{-/-}$ samples. (C) RT-qPCR analysis of histone acetyltransferase (HAT) gene mRNA expression in *Hbo1*$^{+/+}$ and *Hbo1*$^{-/-}$ PEFs. (D) Western blots of total PEF lysate probed for GCN5 and actin. (E) Mean densitometry readings of GCN5 protein levels normalized to actin, showing no significant changes in GCN5 protein in *Hbo1*$^{-/-}$ PEFs. Data are presented as means ± SEM and were analyzed as described in Materials and Methods.

has shown that the quantity of similar essential transcriptional regulators translated from maternally encoded mRNA is insufficient to support the development of embryos beyond the blastocyst stage (64, 73). The observations that *Hbo1*$^{-/-}$ embryos developed well past E4.5 to the 10-somite stage, along with normal proliferation of the inner cell mass outgrowths and fibroblasts, show that HBO1 is not essential for cell proliferation. Similarly, the survival of HBO1-deficient flies to the pupal stage (20) suggests that proliferation can also occur in the absence of HBO1 in flies. In addition, we have shown that both DNA replication and cell cycle progression proceed normally in *Hbo1*$^{-/-}$ cells. Nevertheless, these results do not rule out a nonessential role for HBO1 in DNA replication.

Since the majority of genes that we have examined showed moderate to severe reductions in expression, we propose that the fundamental cause of growth retardation in *Hbo1*$^{-/-}$ embryos stems from deficient gene expression affecting multiple loci. Interestingly, the initial formation of neuroectoderm and mesoderm was normal until E8, but the expression of genes required for subsequent patterning of the somites, heart, and vasculature as well as the neural tube was generally reduced. We note that there are discrepancies between our WMISH data (Fig. 4 and 5) and RT-qPCR data (Fig. 7A to D). In general, the large reductions in gene expression observed in our WMISH experiments were either less pronounced or diminished in our RT-qPCR experiments, possibly due to the following complications. First, we used the same amount of RNA per sample to prepare cDNA. This approach normalized any global reduction in RNA synthesis in the mutant embryos compared to the control embryos and so underrepresents the transcriptional deficiency of the *Hbo1* mutant embryos. It should be noted that substantially less total RNA could be

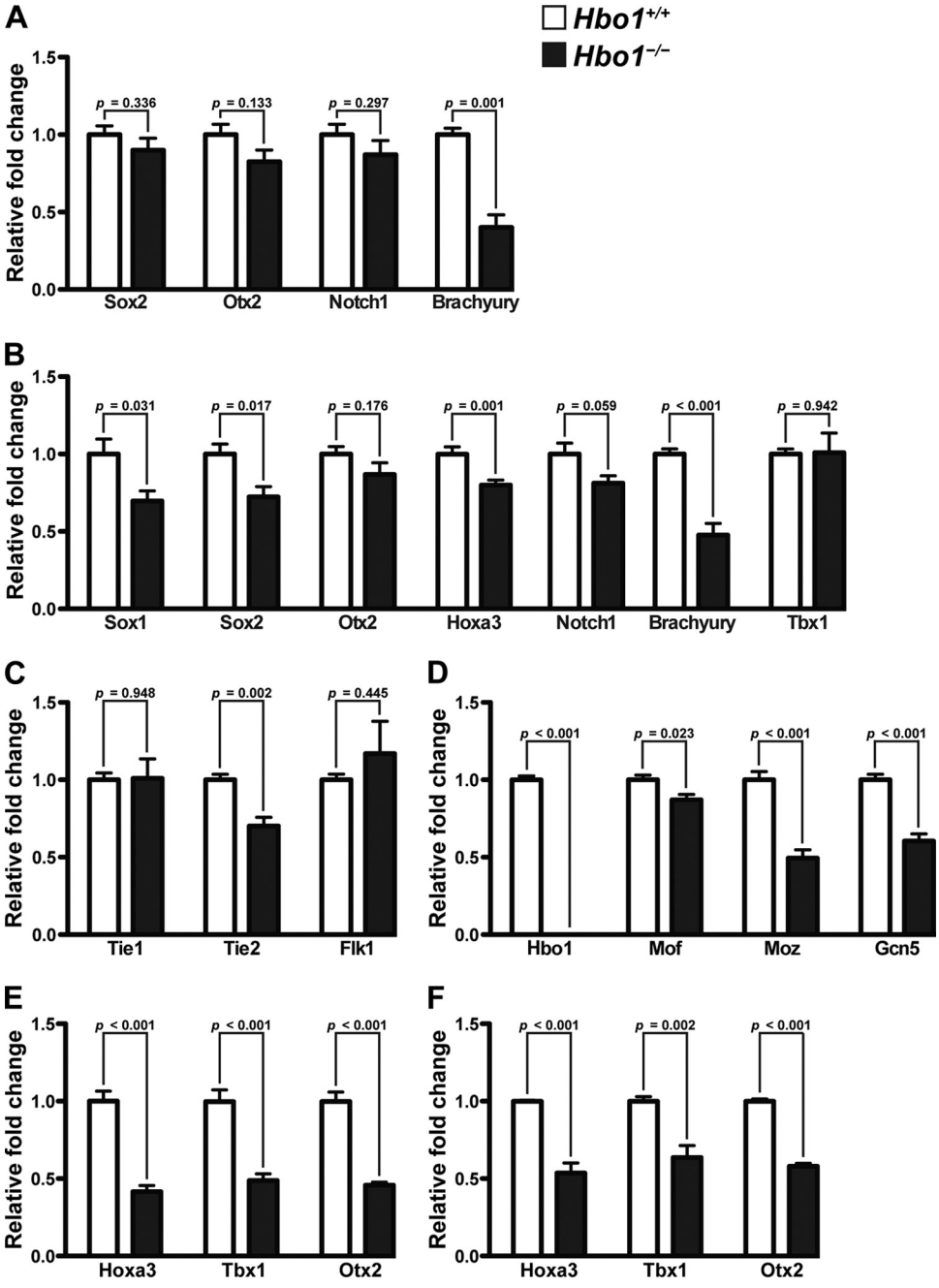

FIG. 7. *Hbo1*$^{-/-}$ embryos feature a general decrease in gene expression at E8.5 and E9.5, along with a reduction of H3K14 acetylation in gene coding regions. (A to D) RT-qPCR analysis of mRNA expression of patterning genes (A and B), vascular genes (C), and HAT genes (D) in stage-matched *Hbo1*$^{+/+}$ and *Hbo1*$^{-/-}$ embryos at E8.5 (A) and E9.5 (B to D). (E and F) ChIP-qPCR analysis of H3K14 acetylation levels in the coding regions of *Hoxa3*, *Tbx1*, and *Otx2* in stage-matched *Hbo1*$^{+/+}$ and *Hbo1*$^{-/-}$ embryos at E8.5 (E) and normalized to H3K14 acetylation levels at *Hsp90ab1* (F).

isolated from the *Hbo1* mutant embryos than from carefully stage-matched controls. Second, as is customary, we have normalized our RT-qPCR data against data for housekeeping genes, including *Hsp90ab1*, *Pgk1*, and *Rpl13a*. As the expression levels of these housekeeping genes were lower in *Hbo1*$^{-/-}$ embryos, normalizations made against housekeeping genes tended to underrepresent differences in gene expression between *Hbo1*$^{-/-}$ embryos and control embryos. Our data suggest that there is a global reduction in gene expression in *Hbo1*$^{-/-}$ embryos. Despite the global reduction in gene expression and despite the fact that this reduction was normalized both at the cDNA synthesis step and during analysis of the qPCR data, certain genes are significantly reduced in the absence of HBO1, showing that they have a greater dependence on HBO1 for normal levels of expression than other genes. Third, the propensity for mesodermal and mesenchymal cell

types to undergo cell death before other cell types (Fig. 2Q and R) skews the cell type composition in *Hbo1*$^{-/-}$ embryos compared to that in controls, resulting in a reduction of mesoderm- and mesenchyme-associated genes over that of other genes. Indeed, this is reflected in our RT-qPCR data, where *brachyury* expression was drastically reduced in comparison to that of the neuronal genes *Sox1*, *Sox2*, and *Otx2*. In contrast, our WMISH experiments showed normal staining intensity for *brachyury* per cell in *Hbo1*$^{-/-}$ embryos, possibly due to the fact that these embryos were less developed than those used in our RT-qPCR experiments. Similarly, while Flk-1 expression appeared to be reduced in *Hbo1*$^{-/-}$ embryos at E8 in the WMISH data, it is possible that the apparent increase in Flk-1 expression seen in the RT-qPCR data could reflect the relative enrichment of vasculature tissue compared to other tissue types in the E9.5 *Hbo1*$^{-/-}$ embryo. We propose that skewed cell type composition in *Hbo1*$^{-/-}$ embryos combined with normalization methods during cDNA synthesis and qPCR data analysis generates the observed discrepancies between WMISH and RT-qPCR results. However, it is important to note that the overall analyses of gene expression in *Hbo1*$^{-/-}$ embryos by WMISH and RT-qPCR are in agreement, with both techniques showing that, in the absence of HBO1, gene expression was generally reduced and no significant increase in expression was detectable for any of the genes examined.

We found that increased apoptosis, particularly affecting mesodermal structures, ultimately led to growth arrest of *Hbo1* null embryos, possibly because the postgastrulation developmental programs of gene expression were unable to support the survival of newly differentiated tissues. In contrast, fibroblasts isolated from embryos lacking HBO1 thrive in culture, indicating that key subsets of genes are expressed at adequate levels in *Hbo1*$^{-/-}$ cells. We conclude from our phenotypic and gene expression analyses that transcriptional activity is sufficient in *Hbo1*$^{-/-}$ embryos until the completion of gastrulation, at which point the maintenance of expression of many genes becomes dependent on HBO1 and a reduction in transcription at multiple essential loci eventually results in cell death and embryonic lethality.

HBO1 has been implicated in the acetylation of H3, H4K5, H4K8, and H4K12 (14, 17, 51). In contrast, we found surprisingly specific changes in histone acetylation in PEFs isolated from *Hbo1* null embryos. Acetylation of H3K14 was 10-fold lower in *Hbo1*$^{-/-}$ PEFs than in wild-type PEFs, whereas H3K9, H4K5, and H4K16 acetylation increased by various degrees. As H4K16 acetylation is entirely dependent on the presence of MOF in early embryos (21, 64) and in cultured HeLa cells (61), the 3-fold increase in H4K16 acetylation in *Hbo1*$^{-/-}$ PEFs is likely to be attributed to the corresponding 37% increase in *Mof* transcripts. Indeed, we did not expect decreases in H4K16 acetylation in *Hbo1*$^{-/-}$ PEFs, as HBO1 does not acetylate H4K16 on recombinant nucleosomes (14). We have shown previously that MOZ displays acetylation activity specific to H3K9, at least at *Hox* loci (69). The fact that *Moz* expression is normal in *Hbo1*$^{-/-}$ PEFs leads us to propose that the observed increases in H3K9 and possibly H4K5 acetylation may be secondary effects arising as a consequence of a primary loss of H3K14 acetylation in *Hbo1*$^{-/-}$ PEFs at the histone level, rather than underlying aberrations in the expression of histone modifiers at the transcriptional level. Our data suggest that acetylated H3K14 may act as a negative regulator of the acetylation of H3K9, H4K5, and H4K16, either directly via steric hindrance or by acting as a docking site for proteins that may ultimately catalyze the removal of these acetylation marks. In all, this supports the theory that extensive cross talk occurs between histone modification marks (16, 23, 31, 36) and highlights the essential contribution of HBO1 in maintaining proper chromatin states.

Taking into account that the only histone residue in *Hbo1*$^{-/-}$ PEFs to display compromised acetylation levels was H3K14, our data strongly suggest that HBO1 is the principal acetyltransferase required for the acetylation of H3K14. In support of this, a 50% or greater reduction in the level of H3K14 acetylation was detected in the coding regions of *Tbx1*, *Otx2*, and *Hoxa3* in E8 *Hbo1*$^{-/-}$ embryos, concomitant with a general depression in the expression of these genes. On the other hand, *Hsp90ab1* acetylation levels were reduced by 24%, and this corresponded to a 30% reduction in *Hsp90ab1* expression in E8 *Hbo1*$^{-/-}$ embryos (data not shown). Overall, these findings suggest that HBO1 and its associated H3K14 acetylation activity are necessary for the normal expression of most genes in a genome-wide context. Evidently, certain genes feature a greater inherent dependency on HBO1-mediated H3K14 acetylation than others.

Although H3K14 acetylation was reduced by more than 10-fold in *Hbo1*$^{-/-}$ PEFs, we observed some persistence of immunoreactivity to acetylated H3K14. This may reflect residual H3K14 acetylation, possibly by mammalian GCN5. *Schizosaccharomyces pombe* Gcn5 (33) and mammalian GCN5 (2) can acetylate H3K14 at gene coding regions to promote transcriptional elongation. However, as GCN5 protein levels were not significantly changed in *Hbo1*$^{-/-}$ PEFs, it is apparent that GCN5-mediated H3K14 acetylation is insufficient to compensate for the absence of HBO1, which further demonstrates the significance of HBO1 for H3K14 acetylation.

Based on the findings that ING4/ING5-containing HBO1 complexes preferentially acetylate histones at transcriptional promoters, whereas HBO1 complexes without ING4/ING5 are targeted by JADE1S to predominantly acetylate histones at downstream gene coding regions, HBO1 acetylation of promoters has been proposed to facilitate transcriptional activation, whereas acetylation of downstream coding regions would promote transcriptional elongation (51). In this respect, it is likely that the primary requirement of most H3K14 acetylation is regulation of gene expression patterns during the complex process of differentiation and lineage specification that occurs after gastrulation, whereas a basal level of H3K14 acetylation is sufficient for basic cell survival and proliferation.

With regard to the existing literature on HBO1 function, our data show discordances associated with cell proliferation, cell cycle progression, DNA replication, and histone acetylation specificity. We note that others have utilized predominantly human cancer cell lines, including HeLa cells, C33A cells, MCF7 cells, Saos2 cells, and A549 cells, to conduct their experiments (26, 27, 29, 43, 44, 75). Evidently, these cell lines are highly abnormal and not ideal for examining normal cell proliferation, cell cycle progression, or DNA replication, due to multiple chromosomal duplications, deletions, frameshift mutations, and inversions within key cell cycle regulatory genes. Furthermore, Iizuka and others have demonstrated that HBO1

is highly upregulated in cancerous cells (29), suggesting that these cells may have acquired an abnormal and complete dependency on HBO1 for basic cellular processes, such as cell proliferation and DNA replication. Lastly, it is also possible that functional redundancy exists in our mouse model and not in human cell lines. However, this is less likely, as HBO1 does not coexist as a highly homologous pair of proteins, as do MOF and TIP60 as well as QKF and MOZ.

In conclusion, we have provided the first *in vivo* characterization of the loss-of-function phenotype of *Hbo1* in mice, revealing a requirement for HBO1 in postgastrulation embryonic development. We show that HBO1 is not required for cell proliferation or DNA replication but instead is an indispensable activator of multiple genes during postgastrulation development. Importantly, we have identified a novel and nonredundant role of HBO1 in promoting the acetylation of H3K14.

ACKNOWLEDGMENTS

This work was funded by the Walter and Eliza Hall Institute and the Australian NHMRC.

We thank C. Gatt, T. McLennan, and N. Downer for excellent technical support. We appreciate the gifts of the recombineering reagents from N. Copeland and of cDNA clones from L. Robb, V. Papaioannou, and T. Willson.

We have no conflicting interests.

REFERENCES

1. **Acampora, D., et al.** 1995. Forebrain and midbrain regions are deleted in Otx2−/− mutants due to a defective anterior neuroectoderm specification during gastrulation. Development **121:**3279–3290.
2. **Agalioti, T., G. Chen, and D. Thanos.** 2002. Deciphering the transcriptional histone acetylation code for a human gene. Cell **111:**381–392.
3. **Akhtar, A., and P. B. Becker.** 2000. Activation of transcription through histone H4 acetylation by MOF, an acetyltransferase essential for dosage compensation in Drosophila. Mol. Cell **5:**367–375.
4. **Biben, C., and R. P. Harvey.** 1997. Homeodomain factor Nkx2-5 controls left/right asymmetric expression of bHLH gene eHand during murine heart development. Genes Dev. **11:**1357–1369.
5. **Bochman, M. L., and A. Schwacha.** 2008. The Mcm2-7 complex has in vitro helicase activity. Mol. Cell **31:**287–293.
6. **Boncinelli, E., and R. Morgan.** 2001. Downstream of Otx2, or how to get a head. Trends Genet. **17:**633–636.
7. **Braunstein, M., A. B. Rose, S. G. Holmes, C. D. Allis, and J. R. Broach.** 1993. Transcriptional silencing in yeast is associated with reduced nucleosome acetylation. Genes Dev. **7:**592–604.
8. **Braunstein, M., R. E. Sobel, C. D. Allis, B. M. Turner, and J. R. Broach.** 1996. Efficient transcriptional silencing in Saccharomyces cerevisiae requires a heterochromatin histone acetylation pattern. Mol. Cell. Biol. **16:**4349–4356.
9. **Burke, T. W., J. G. Cook, M. Asano, and J. R. Nevins.** 2001. Replication factors MCM2 and ORC1 interact with the histone acetyltransferase HBO1. J. Biol. Chem. **276:**15397–15408.
10. **Chapman, D. L., et al.** 1996. Expression of the T-box family genes, Tbx1-Tbx5, during early mouse development. Dev. Dyn. **206:**379–390.
11. **Contzler, R., et al.** 2006. Histone acetyltransferase HBO1 inhibits NF-kappaB activity by coactivator sequestration. Biochem. Biophys. Res. Commun. **350:**208–213.
12. **Dessaud, E., A. P. McMahon, and J. Briscoe.** 2008. Pattern formation in the vertebrate neural tube: a sonic hedgehog morphogen-regulated transcriptional network. Development **135:**2489–2503.
13. **Dhalluin, C., et al.** 1999. Structure and ligand of a histone acetyltransferase bromodomain. Nature **399:**491–496.
14. **Doyon, Y., et al.** 2006. ING tumor suppressor proteins are critical regulators of chromatin acetylation required for genome expression and perpetuation. Mol. Cell **21:**51–64.
15. **Dumont, D. J., et al.** 1994. Dominant-negative and targeted null mutations in the endothelial receptor tyrosine kinase, tek, reveal a critical role in vasculogenesis of the embryo. Genes Dev. **8:**1897–1909.
16. **Fischle, W., Y. Wang, and C. D. Allis.** 2003. Histone and chromatin cross-talk. Curr. Opin. Cell Biol. **15:**172–183.
17. **Foy, R. L., et al.** 2008. Role of Jade-1 in the histone acetyltransferase (HAT) HBO1 complex. J. Biol. Chem. **283:**28817–28826.
18. **Georgiakaki, M., et al.** 2006. Ligand-controlled interaction of histone acetyltransferase binding to ORC-1 (HBO1) with the N-terminal transactivating domain of progesterone receptor induces steroid receptor coactivator 1-dependent coactivation of transcription. Mol. Endocrinol. **20:**2122–2140.
19. **Gridley, T.** 2006. The long and short of it: somite formation in mice. Dev. Dyn. **235:**2330–2336.
20. **Grienenberger, A., et al.** 2002. The MYST domain acetyltransferase Chameau functions in epigenetic mechanisms of transcriptional repression. Curr. Biol. **12:**762–766.
21. **Gupta, A., et al.** 2008. The mammalian ortholog of Drosophila MOF that acetylates histone H4 lysine 16 is essential for embryogenesis and oncogenesis. Mol. Cell. Biol. **28:**397–409.
22. **Hayashi, S., and A. P. McMahon.** 2002. Efficient recombination in diverse tissues by a tamoxifen-inducible form of Cre: a tool for temporally regulated gene activation/inactivation in the mouse. Dev. Biol. **244:**305–318.
23. **Hayashi, Y., T. Senda, N. Sano, and M. Horikoshi.** 2009. Theoretical framework for the histone modification network: modifications in the unstructured histone tails form a robust scale-free network. Genes Cells **14:**789–806.
24. **Hu, Y., et al.** 2009. Homozygous disruption of the Tip60 gene causes early embryonic lethality. Dev. Dyn. **238:**2912–2921.
25. **Huang, L. E., Z. Arany, D. M. Livingston, and H. F. Bunn.** 1996. Activation of hypoxia-inducible transcription factor depends primarily upon redox-sensitive stabilization of its alpha subunit. J. Biol. Chem. **271:**32253–32259.
26. **Iizuka, M., T. Matsui, H. Takisawa, and M. M. Smith.** 2006. Regulation of replication licensing by acetyltransferase Hbo1. Mol. Cell. Biol. **26:**1098–1108.
27. **Iizuka, M., et al.** 2008. Hbo1 links p53-dependent stress signaling to DNA replication licensing. Mol. Cell. Biol. **28:**140–153.
28. **Iizuka, M., and B. Stillman.** 1999. Histone acetyltransferase HBO1 interacts with the ORC1 subunit of the human initiator protein. J. Biol. Chem. **274:**23027–23034.
29. **Iizuka, M., et al.** 2009. Histone acetyltransferase Hbo1: catalytic activity, cellular abundance, and links to primary cancers. Gene **436:**108–114.
30. **Jacobson, R. H., A. G. Ladurner, D. S. King, and R. Tjian.** 2000. Structure and function of a human TAFII250 double bromodomain module. Science **288:**1422–1425.
31. **Jenuwein, T., and C. D. Allis.** 2001. Translating the histone code. Science **293:**1074–1080.
32. **Johmura, Y., S. Osada, M. Nishizuka, and M. Imagawa.** 2008. FAD24 acts in concert with histone acetyltransferase HBO1 to promote adipogenesis by controlling DNA replication. J. Biol. Chem. **283:**2265–2274.
33. **Johnsson, A., et al.** 2009. HAT-HDAC interplay modulates global histone H3K14 acetylation in gene-coding regions during stress. EMBO Rep. **10:**1009–1014.
34. **Katsumoto, T., et al.** 2006. MOZ is essential for maintenance of hematopoietic stem cells. Genes Dev. **20:**1321–1330.
35. **Korhonen, J., et al.** 1992. Enhanced expression of the tie receptor tyrosine kinase in endothelial cells during neovascularization. Blood **80:**2548–2555.
36. **Kouzarides, T.** 2007. Chromatin modifications and their function. Cell **128:**693–705.
37. **Kurdistani, S. K., S. Tavazoie, and M. Grunstein.** 2004. Mapping global histone acetylation patterns to gene expression. Cell **117:**721–733.
38. **Liu, L. X., et al.** 2002. Stabilization of vascular endothelial growth factor mRNA by hypoxia-inducible factor 1. Biochem. Biophys. Res. Commun. **291:**908–914.
39. **Liu, P., N. A. Jenkins, and N. G. Copeland.** 2003. A highly efficient recombineering-based method for generating conditional knockout mutations. Genome Res. **13:**476–484.
40. **Loughran, S. J., et al.** 2008. The transcription factor Erg is essential for definitive hematopoiesis and the function of adult hematopoietic stem cells. Nat. Immunol. **9:**810–819.
41. **Machida, Y. J., J. L. Hamlin, and A. Dutta.** 2005. Right place, right time, and only once: replication initiation in metazoans. Cell **123:**13–24.
42. **Miotto, B., et al.** 2006. Chameau HAT and DRpd3 HDAC function as antagonistic cofactors of JNK/AP-1-dependent transcription during Drosophila metamorphosis. Genes Dev. **20:**101–112.
43. **Miotto, B., and K. Struhl.** 2010. HBO1 histone acetylase activity is essential for DNA replication licensing and inhibited by Geminin. Mol. Cell **37:**57–66.
44. **Miotto, B., and K. Struhl.** 2008. HBO1 histone acetylase is a coactivator of the replication licensing factor Cdt1. Genes Dev. **22:**2633–2638.
45. **Nicosia, R. F., E. Bonanno, M. Smith, and P. Yurchenco.** 1994. Modulation of angiogenesis in vitro by laminin-entactin complex. Dev. Biol. **164:**197–206.
46. **Nye, J. S., R. Kopan, and R. Axel.** 1994. An activated Notch suppresses neurogenesis and myogenesis but not gliogenesis in mammalian cells. Development **120:**2421–2430.
47. **Perez-Campo, F. M., J. Borrow, V. Kouskoff, and G. Lacaud.** 2009. The histone acetyl transferase activity of monocytic leukemia zinc finger is critical for the proliferation of hematopoietic precursors. Blood **113:**4866–4874.
48. **Puri, M. C., J. Rossant, K. Alitalo, A. Bernstein, and J. Partanen.** 1995. The receptor tyrosine kinase TIE is required for integrity and survival of vascular endothelial cells. EMBO J. **14:**5884–5891.
49. **Roh, T. Y., S. Cuddapah, and K. Zhao.** 2005. Active chromatin domains are

defined by acetylation islands revealed by genome-wide mapping. Genes Dev. **19:**542–552.
50. **Rossant, J., and L. Howard.** 2002. Signaling pathways in vascular development. Annu. Rev. Cell Dev. Biol. **18:**541–573.
51. **Saksouk, N., et al.** 2009. HBO1 HAT complexes target chromatin throughout gene coding regions via multiple PHD finger interactions with histone H3 tail. Mol. Cell **33:**257–265.
52. **Sasai, Y.** 2001. Roles of Sox factors in neural determination: conserved signaling in evolution? Int. J. Dev. Biol. **45:**321–326.
53. **Sato, T. N., Y. Qin, C. A. Kozak, and K. L. Audus.** 1993. Tie-1 and tie-2 define another class of putative receptor tyrosine kinase genes expressed in early embryonic vascular system. Proc. Natl. Acad. Sci. U. S. A. **90:**9355–9358.
54. **Schubeler, D., et al.** 2004. The histone modification pattern of active genes revealed through genome-wide chromatin analysis of a higher eukaryote. Genes Dev. **18:**1263–1271.
55. **Schwenk, F., U. Baron, and K. Rajewsky.** 1995. A cre-transgenic mouse strain for the ubiquitous deletion of loxP-flanked gene segments including deletion in germ cells. Nucleic Acids Res. **23:**5080–5081.
56. **Shalaby, F., et al.** 1995. Failure of blood-island formation and vasculogenesis in Flk-1-deficient mice. Nature **376:**62–66.
57. **Sharma, M., M. Zarnegar, X. Li, B. Lim, and Z. Sun.** 2000. Androgen receptor interacts with a novel MYST protein, HBO1. J. Biol. Chem. **275:**35200–35208.
58. **Smith, J.** 1999. T-box genes: what they do and how they do it. Trends Genet. **15:**154–158.
59. **Solloway, M. J., and R. P. Harvey.** 2003. Molecular pathways in myocardial development: a stem cell perspective. Cardiovasc. Res. **58:**264–277.
60. **Strahl, B. D., and C. D. Allis.** 2000. The language of covalent histone modifications. Nature **403:**41–45.
61. **Taipale, M., et al.** 2005. hMOF histone acetyltransferase is required for histone H4 lysine 16 acetylation in mammalian cells. Mol. Cell. Biol. **25:**6798–6810.
62. **Thomas, P. Q., A. Brown, and R. S. Beddington.** 1998. Hex: a homeobox gene revealing peri-implantation asymmetry in the mouse embryo and an early transient marker of endothelial cell precursors. Development **125:**85–94.
63. **Thomas, T., et al.** 2006. Monocytic leukemia zinc finger protein is essential for the development of long-term reconstituting hematopoietic stem cells. Genes Dev. **20:**1175–1186.
64. **Thomas, T., M. P. Dixon, A. J. Kueh, and A. K. Voss.** 2008. Mof (MYST1 or KAT8) is essential for progression of embryonic development past the blastocyst stage and required for normal chromatin architecture. Mol. Cell. Biol. **28:**5093–5105.
65. **Thomas, T., and M. Dziadek.** 1993. Genes coding for basement membrane glycoproteins laminin, nidogen, and collagen IV are differentially expressed in the nervous system and by epithelial, endothelial, and mesenchymal cells of the mouse embryo. Exp. Cell Res. **208:**54–67.
66. **Thomas, T., K. L. Loveland, and A. K. Voss.** 2007. The genes coding for the MYST family histone acetyltransferases, Tip60 and Mof, are expressed at high levels during sperm development. Gene Expr. Patterns **7:**657–665.
67. **Thomas, T., A. K. Voss, K. Chowdhury, and P. Gruss.** 2000. Querkopf, a MYST family histone acetyltransferase, is required for normal cerebral cortex development. Development **127:**2537–2548.
68. **Turner, B. M.** 2000. Histone acetylation and an epigenetic code. Bioessays **22:**836–845.
69. **Voss, A. K., C. Collin, M. P. Dixon, and T. Thomas.** 2009. Moz and retinoic acid coordinately regulate H3K9 acetylation, Hox gene expression, and segment identity. Dev. Cell **17:**674–686.
70. **Voss, A. K., D. L. Krebs, and T. Thomas.** 2006. C3G regulates the size of the cerebral cortex neural precursor population. EMBO J. **25:**3652–3663.
71. **Voss, A. K., T. Thomas, and P. Gruss.** 1997. Germ line chimeras from female ES cells. Exp. Cell Res. **230:**45–49.
72. **Voss, A. K., T. Thomas, and P. Gruss.** 2000. Mice lacking HSP90beta fail to develop a placental labyrinth. Development **127:**1–11.
73. **Voss, A. K., et al.** 2000. Taube nuss is a novel gene essential for the survival of pluripotent cells of early mouse embryos. Development **127:**5449–5461.
74. **Wilkinson, D. G., S. Bhatt, and B. G. Herrmann.** 1990. Expression pattern of the mouse T gene and its role in mesoderm formation. Nature **343:**657–659.
75. **Wu, Z. Q., and X. Liu.** 2008. Role for Plk1 phosphorylation of Hbo1 in regulation of replication licensing. Proc. Natl. Acad. Sci. U. S. A. **105:**1919–1924.